3652486, 0, Downloaded from https://onlinelibrary.wiley.com/doi/10.1111/gcb.16594 by University Of Alaska Fairbanks, Wiley Online Library on [20/01/2023]. See the Terms

## RESEARCH ARTICLE



# Modeled production, oxidation, and transport processes of wetland methane emissions in temperate, boreal, and Arctic regions

```
Masahito Ueyama<sup>1</sup> | Sara H. Knox<sup>2</sup> | Kyle B. Delwiche<sup>3</sup> | Sheel Bansal<sup>4</sup> | William J. Riley<sup>5</sup> | Dennis Baldocchi<sup>3</sup> | Takashi Hirano<sup>6</sup> | Gavin McNicol<sup>7</sup> | Karina Schafer<sup>8</sup> | Lisamarie Windham-Myers<sup>9</sup> | Benjamin Poulter<sup>10</sup> | Robert B. Jackson<sup>11</sup> | Kuang-Yu Chang<sup>5</sup> | Jiquen Chen<sup>12</sup> | Housen Chu<sup>5</sup> | Ankur R. Desai<sup>13</sup> | Sébastien Gogo<sup>14</sup> | Hiroki Iwata<sup>15</sup> | Minseok Kang<sup>16</sup> | Ivan Mammarella<sup>17</sup> | Matthias Peichl<sup>18</sup> | Oliver Sonnentag<sup>19</sup> | Eeva-Stiina Tuittila<sup>20</sup> | Youngryel Ryu<sup>21</sup> | Eugénie S. Euskirchen<sup>22</sup> | Mathias Göckede<sup>23</sup> | Adrien Jacotot<sup>24</sup> | Mats B. Nilsson<sup>18</sup> | Torsten Sachs<sup>25</sup> |
```

are governed by the applicable Creative Commons License

<sup>&</sup>lt;sup>1</sup>Graduate School of Agriculture, Osaka Metropolitan University, Sakai, Japan

<sup>&</sup>lt;sup>2</sup>Department of Geography, The University of British Columbia, Vancouver, Canada

<sup>&</sup>lt;sup>3</sup>Department of Environmental Science, Policy & Management, UC Berkeley, Berkeley, California, USA

<sup>&</sup>lt;sup>4</sup>U.S. Geological Survey, Northern Prairie Wildlife Research Center, Jamestown, North Dakota, USA

<sup>&</sup>lt;sup>5</sup>Climate and Ecosystem Sciences Division, Lawrence Berkeley National Laboratory, Berkeley, California, USA

<sup>&</sup>lt;sup>6</sup>Research Faculty of Agriculture, Hokkaido University, Sapporo, Japan

<sup>&</sup>lt;sup>7</sup>Department of Earth and Environmental Sciences, University of Illinois Chicago, Chicago, Illinois, USA

<sup>&</sup>lt;sup>8</sup>Department of Earth and Env Science, Rutgers University Newark, New Jersey, USA

<sup>&</sup>lt;sup>9</sup>Water Mission Area, U.S. Geological Survey, Menlo Park, California, USA

<sup>&</sup>lt;sup>10</sup>NASA Goddard Space Flight Center, Biospheric Sciences Laboratory, Greenbelt, Maryland, USA

<sup>&</sup>lt;sup>11</sup>Department of Earth System Science, Stanford University, Stanford, California, USA

<sup>&</sup>lt;sup>12</sup>Department of Geography, Environment, and Spatial Sciences, Michigan State University, East Lansing, Michigan, USA

<sup>&</sup>lt;sup>13</sup>Dept of Atmospheric and Oceanic Sciences, University of Wisconsin-Madison, Madison, Wisconsin, USA

<sup>&</sup>lt;sup>14</sup>ECOBIO (Écosystèmes, Biodiversité, Évolution), Université Rennes 1, CNRS UMR 6553, Rennes, France

<sup>&</sup>lt;sup>15</sup>Department of Environmental Science, Faculty of Science, Shinshu University, Matsumoto, Japan

<sup>&</sup>lt;sup>16</sup>National Center for Agro Meteorology, Seoul, South Korea

 $<sup>^{17}</sup> Institute for Atmospheric and Earth System Research/Physics, Faculty of Science, University of Helsinki, Helsinki, Finland Control of C$ 

<sup>&</sup>lt;sup>18</sup>Department of Forest Ecology and Management, Swedish University of Agricultural Sciences, Umeå, Sweden

<sup>&</sup>lt;sup>19</sup>Université de Montréal, Département de géographie, Université de Montréal, Montréal, Quebec, Canada

<sup>&</sup>lt;sup>20</sup>School of Forest Sciences, University of Eastern Finland, Joesnuu, Finland

 $<sup>^{21}</sup>$ Department of Landscape Architecture and Rural Systems Engineering, Seoul National University, Seoul, South Korea

<sup>&</sup>lt;sup>22</sup>University of Alaska Fairbanks, Institute of Arctic Biology, Fairbanks, Alaska, USA

<sup>&</sup>lt;sup>23</sup>Max Planck Institute for Biogeochemistry, Department of Biogeochemical Signals, Jena, Germany

<sup>&</sup>lt;sup>24</sup>INRAE, UMR 1069 SAS, Rennes, France

<sup>&</sup>lt;sup>25</sup>GFZ German Research Centre for Geosciences, Telegrafenberg, Potsdam, Germany



#### Correspondence

Masahito Ueyama, Graduate School of Agriculture, Osaka Metropolitan University, Sakai, Japan.

Email: mueyama@omu.ac.jp

### **Funding information**

Arctic Challenge for Sustainability II. Grant/Award Number: JPMXD1420318865; Arctic Observatory Program of the National Science Foundation, Grant/Award Number: 1936752, 1503912 and 1107892; Bonanza Creek Long-Term Ecological Research Program funded by the National Science Foundation, Grant/Award Number: NSF DFB-1026415 and DFB-1636476: California Department of Water Resources, CA Fish and Wildlife; Canada Research Chairs, Canada Foundation for Innovation Leaders Opportunity Fund: ICOS-Finland, Grant/Award Number: 3119871: JSPS KAKENHI. Grant/Award Number: 20K21849; Ministry of Environment of Korea, Grant/ Award Number: 2022003640002; Natural Sciences and Engineering Research Council Discovery Grant Programs; NSF Long-Term Research in Environmental Biology Program, Grant/Award Number: NSF LTREB 2011276; Reducing Uncertainties in Biogeochemical Interactions through Synthesis and Computation (RUBISCO) Scientific Focus Area, Office of Biological and Environmental Research of the U.S. Department of Energy Office of Science; Rural Development Administration, Grant/Award Number: PJ014892022022; SNO Tourbières, CNRS-INSU: U.S. Department of Energy, Grant/Award Number: DE-AC02-05CH11231; U.S. Geological Survey, Ecosystems Mission Area, Land Change Science Program; US DOE Ameriflux, Grant/Award Number: 7544821; US Geological Survey, Research Work, Grant/Award Number: Order 224; Helmholtz Association of German Research Centres, Grant/Award Number: VH-NG-821; Academy of Finland project N-PERM, Grant/Award Number: 341348; Horizon Europe project GreenFeedBack. Grant/Award Number: 101056921: U.S. Geological Survey, John Wesley Powell Center for Analysis and Synthesis; U.S. Geological Survey, Water Mission Area, Earth Systems Processes Division

#### Abstract

Wetlands are the largest natural source of methane (CH<sub>4</sub>) to the atmosphere. The eddy covariance method provides robust measurements of net ecosystem exchange of CH<sub>4</sub>, but interpreting its spatiotemporal variations is challenging due to the cooccurrence of CH<sub>4</sub> production, oxidation, and transport dynamics. Here, we estimate these three processes using a data-model fusion approach across 25 wetlands in temperate, boreal, and Arctic regions. Our data-constrained model—iPEACE—reasonably reproduced CH<sub>4</sub> emissions at 19 of the 25 sites with normalized root mean square error of 0.59, correlation coefficient of 0.82, and normalized standard deviation of 0.87. Among the three processes, CH<sub>4</sub> production appeared to be the most important process, followed by oxidation in explaining inter-site variations in CH<sub>4</sub> emissions. Based on a sensitivity analysis, CH<sub>4</sub> emissions were generally more sensitive to decreased water table than to increased gross primary productivity or soil temperature. For periods with leaf area index (LAI) of ≥20% of its annual peak, plant-mediated transport appeared to be the major pathway for CH<sub>4</sub> transport. Contributions from ebullition and diffusion were relatively high during low LAI (<20%) periods. The lag time between  $CH_A$  production and  $CH_A$  emissions tended to be short in fen sites (3  $\pm$  2 days) and long in bog sites ( $13 \pm 10$  days). Based on a principal component analysis, we found that parameters for CH<sub>4</sub> production, plant-mediated transport, and diffusion through water explained 77% of the variance in the parameters across the 19 sites, highlighting the importance of these parameters for predicting wetland CH₄ emissions across biomes. These processes and associated parameters for CH<sub>4</sub> emissions among and within the wetlands provide useful insights for interpreting observed net CH<sub>4</sub> fluxes, estimating sensitivities to biophysical variables, and modeling global CH<sub>4</sub> fluxes.

## KEYWORDS

 $Bayesian\ optimization,\ data-model\ fusion,\ Eddy\ covariance,\ methane\ emissions,\ methane\ model,\ multi-site\ synthesis$ 

# 1 | INTRODUCTION

Wetlands are the largest natural source of methane ( $CH_4$ )—a potent greenhouse gas contributing to climate warming. Methane emissions from wetlands contribute approximately 20% of total annual  $CH_4$  emissions (Saunois et al., 2020). Despite their importance, estimates of wetland  $CH_4$  emissions are highly uncertain (Bohn et al., 2015; Melton et al., 2013) because direct

measurements of  $\mathrm{CH_4}$  emissions (Delwiche et al., 2021) are far fewer than those of carbon dioxide ( $\mathrm{CO_2}$ ) fluxes (Pastorello et al., 2020). In particular, the variability in  $\mathrm{CH_4}$  emissions appears high across spatial and temporal scales (Delwiche et al., 2021; Knox et al., 2019). As a result of the associated uncertainties, current estimates of the global  $\mathrm{CH_4}$  budget contain large discrepancies between top-down and bottom-up approaches (Jackson et al., 2020; Saunois et al., 2020).

Methane emissions from wetlands also exhibit a wide range of magnitudes and responses to biophysical variables. Because CH<sub>4</sub> is primarily produced by anaerobic methanogens and oxidized by aerobic bacteria (Bridgham et al., 2013; Conrad, 2009), water table depth (WTD) has been identified as an important thermodynamic boundary and thus potential predictor of wetland CH<sub>4</sub> emissions (Brown et al., 2014; Moore & Roulet, 1993; Rinne et al., 2018). Methanogens produce CH<sub>4</sub> using substrates both from carbon recently fixed through photosynthesis (Whiting & Chanton, 1993) and previously fixed carbon (Glaser et al., 2004; Karofeld & Tónisson, 2014). Thus, CH<sub>4</sub> emissions are often correlated with plant primary production and/or soil respiration (Turetsky et al., 2014; Villa et al., 2020; Whiting & Chanton, 1993). Because temperature affects CH₁ production kinetics, soil temperature is typically correlated with CH<sub>4</sub> emissions (Knox et al., 2019; Yvon-Durocher et al., 2014), albeit substantial seasonal hysteresis was reported to occur in many sites, likely due to substrate-temperature driver interactions (Chang et al., 2020, 2021). In addition to production and oxidation, transport pathways are also crucial in modeling CH<sub>4</sub> emissions. Because CH<sub>4</sub> in soils is transported through plant aerenchyma, ebullition bubbles through standing water, and/or diffusion, CH<sub>4</sub> emissions were shown to be often correlated with leaf area index (LAI), latent heat flux, and/or barometric pressure (PA) (Kwon et al., 2017; Sturtevant et al., 2016; Tokida et al., 2005; Ueyama, Hirano, & Kominami, 2020; Ueyama, Yazaki, et al., 2020). To better understand wetland CH<sub>4</sub> emissions, the eddy covari-

ance (EC) method has been widely used at various wetlands along with measurements of other ancillary covariates such as WTD and soil temperature (Delwiche et al., 2021; Knox et al., 2019; Morin, 2018). The EC method provides quasi-continuous measurements of CH<sub>4</sub>, CO<sub>2</sub>, and energy exchanges between the land surface and the atmosphere (Baldocchi, 2014). The direct measurements have been used to evaluate magnitudes of CH<sub>4</sub> emissions, their interannual variations, and their responses to various biophysical variables (Chang et al., 2021; Chu et al., 2014; Knox et al., 2019; Rinne et al., 2018; Yuan et al., 2022). Previous studies have identified biophysical variables such as soil and air temperature and WTD as the primary drivers for the temporal and spatial variations in CH<sub>4</sub> emissions (Knox et al., 2019; Turetsky et al., 2014; Yuan et al., 2022), but their importance varies substantially among wetlands and across time scales (Knox et al., 2021; Koebsch et al., 2015). Furthermore, complex interactions hinder the use of simple correlation analyses for disentangling responses of CH<sub>4</sub> emissions to biophysical variables, leading to large uncertainties when interpreting observations (Chang et al., 2020; Knox et al., 2021; Sturtevant et al., 2016). Recently, the FLUXNET-CH database was curated for supporting synthesis of wetland CH<sub>4</sub> emissions using the EC methods (Delwiche et al., 2021; Knox et al., 2019) and, for example, was used to evaluate inter-site variations in CH<sub>4</sub> emissions (Chang et al., 2021; Knox et al., 2021; Yuan et al., 2022).

To improve the mechanistic understanding and accurate modeling of  $CH_4$  emissions, the relative contributions of  $CH_4$  emission

pathways have been measured or estimated with various field measurements (Table 1). These measurements include chamber techniques (Korrensalo et al., 2022; Tokida, Miyazaki, et al., 2007; Tokida, Mizoguchi, et al., 2007), bubble traps (Stanley et al., 2019), isotope techniques (Dorodnikov et al., 2011), and dissolved CH<sub>4</sub> concentrations in pore water (McNicol et al., 2017). Recently, a wavelet analysis of EC measurements examined the contribution of ebullition to total CH<sub>4</sub> emissions (Göckede et al., 2019; Iwata et al., 2018; Hwang et al., 2020; Richardson et al., 2022; Schaller et al., 2019). These analyses revealed that plant-mediated transport was the most important pathway for wetland CH<sub>4</sub> emissions (up to 98% of the total emissions), but the other two pathways were also important under environmental conditions such as flooded wetlands without emergent vegetation and shallow ponds. Many process-based models (Table 1) have also shown that CH<sub>4</sub> emissions occur mostly through plant-mediated transport (Castro-Morales et al., 2018; Ma et al., 2017; Peltola et al., 2018; Susiluoto et al., 2018; Wania et al., 2010), although one model found ebullition was the dominant pathway (Ito, 2019). Although previous studies conducted across relatively few wetland sites are useful for understanding CH<sub>4</sub> transport pathways, comparisons of transport mechanisms across multiple wetlands remain challenging. The challenge lies in uncertainties in measurement techniques, spatial representation of measured processes in the field, and different model structures in process-based models.

Data-model fusion approaches have recently been used for evaluating wetland CH<sub>4</sub> emissions (Ma et al., 2017; Müller et al., 2015; Salmon et al., 2022; Susiluoto et al., 2018; Ueyama et al., 2022). These methods use observed data for constraining process-based models that are often difficult to calibrate, and can be used to evaluate processes of CH<sub>4</sub> emissions and their sensitivity to biophysical drivers. To reduce the uncertainties in a process-based model, Müller et al. (2015) used observed data for constraining a model for CH<sub>4</sub> dynamics and found that detailed process-based models were not well constrained owing to the complexity of the model. Susiluoto et al. (2018) calibrated a detailed model using 9 years of EC-based CH<sub>4</sub> flux data in a northern fen. Their results suggested that CH<sub>4</sub> production was the most important factor responsible for the interannual variations in CH<sub>4</sub> emissions, whereas plant-mediated transport was the most important CH<sub>4</sub> transport pathway. Datamodel fusion approaches to study CH<sub>4</sub> emissions have been applied only for a limited number of individual sites; thus, their applicability should be evaluated across wide arrays of wetland sites and biomes.

Recently, Ueyama et al. (2022) developed a process-based model (i.e., inferring Processes for Ecosystem-Atmosphere  $CH_4$  Exchange—iPEACE) for partitioning  $CH_4$  emissions using a data-model fusion approach for a cool temperate bog in Japan. Their approach constrained the model using  $CH_4$  emissions and associated biophysical variables from the EC tower with the goal to determine a parameter set for reproducing daily  $CH_4$  emissions under various environmental conditions. These conditions included growing and dormant seasons, wet and dry conditions, high and low LAI, and various ranges of gross primary production (GPP), soil temperature, and PA. The

	b.	Ġ
۰	2	
	٥	)
	č	)
	Ē	
-	c	5
	2	5
	ŭ	2
	Š	
•	Ĕ	;
	7	5
	Ž	,
	å	)
-	٩	2
		5
-	<u>م</u>	5
:	Ĕ	Ė
	2	
	5	)
	a	5
	ASE	,
	Ċ	2
	F	5
	r	5
	$\mathbf{c}$	2
	ransı	í
	2	2
	+	5
	0	5
	t	5
•	ŧ	5
	٩	)
	ant-m	
	Ė	
-	-	5
	2	2
	ב	5
	Jue 1	5
	_	•
	ē	5
•	5	5
	F	-
	Ξ	5
	č	
	≧	5
	Ξ	
	Ξ	5
-	5	2
	u	
	٩	j
:	=	:
	2	5
	F	
	π	5
	Wet	)
	rom	
	5	)
	Ξ	
	č	-
		١.
	$\overline{c}$	-
	CISS	5
•	nissin	
•	emissin	
	) emission	4, <
		4
-		_
-		4
-	( H	4
-		4
-	ane (CH.)	4
_	ane (CH.)	4
_	d methane (CH.)	4,
	ned methane (CH.)	4,
	ned methane (CH.)	4,
	ned methane (CH.)	4,
	rtitioned methane (CH.)	4,
	nartitioned methane (CH.)	4,
	artitioned methane (CH.)	4, 10, 0, 110, 110, 10, 10, 10, 10, 10, 1
	r nartifioned methane (CH.)	4, 10, 0, 110, 110, 10, 10, 10, 10, 10, 1
	v tor partitioned methane (( H.)	4, 10, 0, 110, 110, 10, 10, 10, 10, 10, 1
	rvev for partitioned methane (CH.)	4. 101 paragraph of 101 /51
	rvev for partitioned methane (CH.)	4. 101 paragraph of 101 /51
	e sirvey for partitioned methane (CH.)	to local managed and to to to
	rvev for partitioned methane (CH.)	the second of th
	e sirvey for partitioned methane (CH.)	the second of th
	e sirvey for partitioned methane (CH.)	deal of the first control of 147
	atilise siirvev tor partitioned methane (CH.)	/b (b )
	eratiire siirvev tor nartitioned methane (CH.)	(d. 19)
	Iteratiire siirvev tor partitioned methane (CH.)	(A) (C) (C) (C) (C) (C) (C) (C) (C) (C) (C
	1   Interatiire siirvev tor partitioned methane (CH.)	/t
	F 1   Herafilire silrvey for partitioned methane (CH.)	/t) \ \ \ \ \ \ \ \ \ \ \ \ \ \ \ \ \ \
	F 1   Iteratiire siirvev tor nartitioned methane (CH.)	(A. 1)
	F 1   Iteratiire siirvev tor nartitioned methane (CH.)	/t) \ \ \ \ \ \ \ \ \ \ \ \ \ \ \ \ \ \

Obs./model	Wetland type	Site	Ebullition	Diffusion	Plant	Method	Period	Reference
Observation	Arctic tundra				92-98	Chamber	Summer	Morrissey and Livingston (1992)
Observation	Arctic tundra				66 (polygon center) 27 (polygon rim)	Chamber	August	Kutzback et al. (2004)
Observation	Arctic tundra	RU-Ch2	2		25 (wet sites) 0 (dry sites)	Chamber	Summer	Kwon et al. (2017)
Observation	Boreal bog	FI-Si2	2-8		31	Bubble trap Chamber	Growing season	Männistö et al. (2019) Korrensalo et al., 2022
Observation	Boreal fen	FI-Sii			21	Chamber		Korrensalo et al. (2022)
Observation	Boreal fen				38 (hummocks) 31 (lawns) 51 (hollows)	<sup>14</sup> C pulse labeling of mesocosms	12 days	Dorodnikov et al. (2011)
Observation	Temperate bog	JP-Bby	50			Chamber	Summer	Tokida, Miyazaki, et al. (2007) and Tokida, Mizoguchi, et al. (2007)
Observation	Temperate bog		14-16			Bubble trap	Growing season	Stamp et al. (2013)
Observation	Temperate bog				64-90	Chamber	May-December	Shannon et al. (1996)
Observation	Temperate fen		38			Bubble trap	Spring & summer	Stanley et al. (2019)
Observation	Temperate fen		~10			Eddy covariance for isoflux	Two days in summer	Santoni et al. (2012)
Observation	Temperate fen (Eriophorum vaginatum)	FR-LGt	54.7 in May 40.7 in March			Chamber	Two months	Gogo et al. (2011)
	Temperate fen ( <i>Sphagnum</i> spp. & <i>Betula</i> spp.)		negligible					
Observation	Temperate marsh (open water)	US-Myb	~1.3	~4.1		Combined eddy covariance and process study Bubble trap in open water area within the flux footprint Gas concentration in water for open water area	Annual	McNicol et al. (2017)
Observation	Temperate marsh (open water)		50	20	Not consier	Chamber at water surface not including vegetation	September	Villa et al. (2021)
Observation	Temperate marsh (floating vegetation)		50	20	Not consier	Chamber at water surface not including vegetation		
Observation	Temperate marsh (emergent vegetation)		66	1	Not consier	Chamber at water surface not including vegetation		
Observation	Temperate marsh (emergent vegetation)	US-Tw1	10-30			Static chambers	Aug. 29- Sep. 2	Windham-Myers et al. (2018)
Observation	Rice paddy		6			Eddy covariance + Wavelet analysis	Growing season	Richardson et al. (2022)

TABLE 1 (Continued).

Obs./model	Obs./model Wetland type	Site	Ebullition	Diffusion Plant	Plant	Method	Period	Reference
Observation	Rice paddy	KR-Crk	10-17			Eddy covariance + Wavelet analysis	Growing season	Hwang et al. (2020)
Observation	Rice paddy			marginal	06-09	Chamber	Growing season	Butterbach-Bahl et al. (1997)
Observation	Rice paddy		4	marginal	96	Chamber	Growing season	Kajiura and Tokida (2021)
Model	pan-Arctic wetland (regional mean)		51.5	<b>T</b>	47.5	VISIT	Annual	Ito (2019)
Model	Boreal bog		9.0	3.4	96	TECO calibrated with chamber data	Annual	Ma et al. (2017)
Model	Boreal fen	FI-Sii	0	37	63	HIMMELI calibrated with eddy covariance data	Annual	Peltola et al. (2018)
Model	Boreal fen	FI-Sii	5	30	75-95	sqHIMMELI calibrated with eddy covariance data	Annual	Susiluoto et al. (2018)
Model	Arctic Tunder near RU-Ch2		4.2	34.8	61.0	JSBACH-methane	Annual	Castro-Morales et al. (2018)
Model	Alpine tundra (Ruoergai)		0.3	28.8	70.8	LPJ-WHyMe v 1.3.1	Annual	Wania et al. (2010)
Model	Subarctic mire (Abisko)		0	15.5	84.5	LPJ-WHyMe v 1.3.1	Annual	Wania et al. (2010)
Model	Boreal fen (BOREAS)		6.0	29.2	66.6	LPJ-WHyMe v 1.3.1	Annual	Wania et al. (2010)
Model	Boreal fen (Salmisuo)		1.4	30.9	67.8	LPJ-WHyMe v 1.3.1	Annual	Wania et al. (2010)
Model	Boreal fen (Degero)		0.8	25.7	74.3	LPJ-WHyMe v 1.3.1	Annual	Wania et al. (2010)
Model	Temperate bog (Michigan)		0	24.4	75.6	LPJ-WHyMe v 1.3.1	Annual	Wania et al. (2010)
Model	Temperate fen (Minnesota)		0.4	22.9	76.7	LPJ-WHyMe v 1.3.1	Annual	Wania et al. (2010)
Model	Temperate fen	US-Los	0.0	23.7	76.3	ORCHIDEE-PEAT revision 7020	Annual	Salmon et al. (2022)
Model	Boreal bog	US-Bzb	0.0	6:0	99.1	ORCHIDEE-PEAT revision 7020	Annual	Salmon et al. (2022)
Model	Temperate fen	FR-LGt	0.0	-0.1	100.1	ORCHIDEE-PEAT revision 7020	Annual	Salmon et al. (2022)
Model	Boreal fen	FI-Lom	0.8	-1.6	100.8	ORCHIDEE-PEAT revision 7020	Annual	Salmon et al. (2022)
Model	Temperate marsh	US-Wpt	0.0	0.0	100.0	ORCHIDEE-PEAT revision 7020	Annual	Salmon et al. (2022)

model reasonably identified processes that were qualitatively consistent with previous field experiments to shed light on processes in the bog. Findings include: (1) ebullition and plant-mediated transport as the important  $CH_4$  transport pathways, (2) high contributions of the deep organic layer (i.e., <30 cm) to total  $CH_4$  emissions due to very low  $CH_4$  concentrations in the surface organic layer (Tokida, Miyazaki, et al., 2007), and (3) gaseous-bubble accumulation in deep organic layer (Tokida et al., 2005; Tokida, Miyazaki, et al., 2007; Tokida, Mizoguchi, et al., 2007). A chamber-based study further suggested that contributions of bubble transport to total  $CH_4$  emissions ranged from 67%–95% during the snow-free season in the bog (Tokida et al., 2005; Tokida, Miyazaki, et al., 2007; Tokida, Mizoguchi, et al., 2007), which was close to the iPEACE model estimates (64%).

Here, we modified iPEACE to simulate  $\mathrm{CH_4}$  fluxes and infer processes related to  $\mathrm{CH_4}$  emissions (i.e., production, oxidation, and transport pathways) from 25 wetlands across mid- to high-latitudes included in the FLUXNET-CH<sub>4</sub> database. Applying the data-model fusion method (Ueyama et al., 2022) across these wetland sites spanning temperate, boreal, and Arctic regions, our objectives were to: (1) evaluate the model's suitability for simulating  $\mathrm{CH_4}$  emissions across wetland types, (2) quantify inter-site variations in estimated processes related to  $\mathrm{CH_4}$  emissions, (3) evaluate the sensitivities of  $\mathrm{CH_4}$  emissions to GPP, soil temperature, and WTD, and (4) examine inter-site variations in parameters for improved predictions of wetland  $\mathrm{CH_4}$  emissions.

#### 2 | MATERIALS AND METHODS

## 2.1 Dataset and model inputs

We used daily EC  $\mathrm{CH_4}$  flux data archived in the FLUXNET- $\mathrm{CH_4}$  database (Delwiche et al., 2021). We selected all mid- to high-latitude freshwater wetland sites from the database (Table 2) that contained all relevant forcing variables (i.e., soil and air temperature, WTD, PA, and GPP). The selected 25 sites represent wetland types of bog (ombrotrophic), fen (minerotrophic), marsh, wet tundra, and rice paddy in temperate, boreal, and Arctic regions. The mean annual air temperature ranged from  $-5^{\circ}\mathrm{C}$  to  $17^{\circ}\mathrm{C}$  across the sites, and minimum WTD ranged from -0.62 to  $0.68\,\mathrm{m}$ .

We used daily gap-filled  ${\rm CH_4}$  fluxes and the ancillary biophysical variables at the tower sites. The daily mean values of the gap-filled half-hourly variables were provided in the FLUXNET-CH $_4$  database (Delwiche et al., 2021). We used two types of daily  ${\rm CH_4}$  fluxes (i.e., FCH4\_F and FCH4\_F\_ANN\_median) in the database. FCH4\_F was gap-filled using a multidimensional scaling (MDS) approach in REddyProc (Delwiche et al., 2021), but still contained periods of time with long data gaps (<2 months). FCH4\_F\_ANN\_median was gap-filled based on an artificial neural network method, which fills all data gaps (Knox et al., 2019). As input drivers from the FLUXNET-CH $_4$  database, daytime-based GPP (GPP\_DT) in the database (Lasslop et al., 2010), air temperature (TA\_F), barometric pressure (PA\_F), soil temperature (TS), and WTD (WTD\_F) were used. The gaps in the

meteorology (i.e., TA\_F, and PA\_F) were filled using the ERA-Interim reanalysis data (Vuichard & Papale, 2015), whereas those of WTD and soil temperatures were filled using the MDS method. We used soil temperature at two depths for representing the surface and deep layers in the model. For sites affected by permafrost (RU-Ch2, US-Ics, and US-Uaf), we assumed that the deepest soil temperature measurement was representative of the bottom of the active layer. Data for RU-Ch2, US-Ics, US-Bzf, and US-Bzb sites did not include WTD data in the FLUXNET-CH<sub>4</sub> database, but WTD data were directly provided from principal investigators. Since WTD for RU-Ch2 was based on discrete manual measurements, we linearly interpolated the data to the daily timescale.

We prepared daily LAI as a model input based on satellite-based LAI smoothed using GPP. First, the four-day LAI data (MCD15A3H; collection 6) was downloaded from MODIS land products subsets. The spatial resolution of the product is 500 m. We used a single grid cell of data centered on the site location. The LAI data were first set to zero for the snow periods, and were then smoothed using a Savitzky-Golay filter (Chen et al., 2004). The snow conditions were determined based on the MODIS reflectance products (MCD43A4; collection 6) from the MODIS land products subsets. Because smoothed LAI often failed to explain seasonal peaks when peak LAI was missing, daily LAI was then modeled using the smoothed LAI and daily GPP normalized with a maximum GPP (nGPP). LAI at day (i) was modeled with a non-centered moving mean of the normalized GPP multiplying a scale factor,

$$LAI_{i} = L_{s} \sum_{j=i-D}^{i} nGPP_{j} / (D+1).$$
 (1)

Two empirical parameters of the scale factor for explaining maximum LAI ( $L_s$ ) and moving window for explaining a lag between GPP and LAI (D) were the parameters determined based on a differential evolution method. Since there was no clear relationship between LAI and GPP for NZ-Kop, LAI for NZ-Kop was estimated simply based on 10-day moving mean of the satellite-based LAI. The smoothed LAI well mimicked the satellite-derived LAI, where mean and standard deviation of root mean square error (RMSE) and correlation coefficient (R) were  $0.46\pm0.24$  and  $0.84\pm0.11$ , respectively, across the sites.

## 2.2 | The iPEACE model

Partitioning  $\mathrm{CH_4}$  emissions from the EC measurements was conducted by the optimization of a process-based model with the data. We used the iPEACE model (Ueyama et al., 2022), which was originally proposed to infer  $\mathrm{CH_4}$  dynamics at a temperate bog in Japan, but has been generalized for the current analysis (Figure 1).

The iPEACE model consists of two soil layers, a surface layer susceptible to oxic conditions and a deep layer prone to anoxic conditions, and considers CH<sub>4</sub> production and oxidation in each layer, as well as three transport pathways: plant-mediated transport, ebullition, and diffusion. The modeled mechanisms are similar to those

TABLE 2 Description of study sites, showing wetland type, location, dominant vegetation type (DOM\_VEG), mean annual air temperature (TAVE), GPP, annual maximum monthly leaf area index (LAI) (MCD15A3H), mean annual soil temperature (T<sub>S</sub>), water table depth during the period when soil was thaw (WTD gs), and modeled partitioned methane (CH<sub>4</sub>) emissions during the growing season when LAI was higher than 20% of the annual maximum.

																-	GIOD		mei i	ge L	71010	97	* 1	, 11	-L I
References	Goeckede (2020)	Euskirchen et al. (2020)	Knox et al. (2019)	Lohila et al. (2020)	Iwata et al. (2020)	Euskirchen and Edgar (2020a)	Euskirchen and Edgar (2020b)	Nilsson and Peichl (2020)	Vesala, Tuittila, Mammarella, and Alekseychik (2020)	Vesala, Tuittila, Mammarella, and Rinne (2020)	Sonnentag and Helbig (2020)	Koebsch and Jurasinski (2020)	Sachs and Wille (2020)	Schmid and Klatt (2020)	Jacotot et al. (2020)	Desai (2020)	Ueyama, Hirano, and Kominami (2020)	Chen and Chu (2020)	Ryu et al. (2020)	Valach et al. (2020)	Eichelmann et al. (2020)	Matthes et al. (2020)	Shortt et al. (2020)	Iwata (2020)	Campbell and Goodrich (2020)
Diffusion (%)	1	0	47	0	12	;	4	5	17	0	11	1	1	ı	1	0	2	1	0	29	0	24	1	23	0
Plant (%)	49	9	53	77	70	;	31	84	29	91	78	1	1	1	87	91	20	1	39	45	22	28	ı	9	70
Ebullition (%)	50	35	0	23	18		89	12	16	6	11	1	1	1	12	6	27	1	61	26	42	18	1	12	30
End year	2015	2016	2015	2010	2018	2016	2016	2018	2016	2018	2017	2018	2018	2014	2018	2018	2018	2013	2018	2018	2018	2018	2018	2012	2015
	2014 2	2015 2	2014 2	2006 2	2011 2	2015 2	2014 2		2012 2	2013 2	2014 2		2013 2			2014 2				2011 2	2013 2	2010 2	2016 2	2012 2	2012 2
Start year	20	20	20	20	20	20	20	2014	200	200	20	2011	20	2012	2017	20	2015	2011	2015	20	20	20	20	20	20
WTD min (m)	-0.02	-0.02	0.09	-0.04	-0.42	-0.01	0.00	-0.29	-0.07	-0.17	-0.37	-0.62	-0.12	-0.24	-0.46	-0.45	-0.23	0.14	0.00	-0.48	-0.37	0.68	-0.58	-0.03	-0.29
WTD gs (m)	-0.01	-0.01	0.09	0.02	-0.14	0.00	0.02	-0.01	0.09	0.03	-0.16	-0.27	0.23	-0.07	-0.23	-0.11	-0.02	0.38	0.01	0.30	0.23	1.23	0.10	-0.01	-0.10
T <sub>s</sub> (°C)	-5.0	-0.8	0.2	3.9	-3.0	4.7	6.4	4.8	9.9	6.2	4.6	10.6	10.9	7.8	10.5	5.4	6.6	13.4 (	11.5 (	12.4	15.3	16.4	16.9	14.5	12.4
	'	1	0	က	1	4	4	4	9	9	4	Ţ	Ţ	7	1	2	6	1	1	1	1	1	1	Ţ	1
LAI (m <sup>2</sup> m <sup>-2</sup> )	2.0	1.7	1.4	2.0	1.4	2.3	1.5	2.2	2.2	2.4	2.9	4.9	2.8	2.9	4.6	6.5	2.7	2.8	2.0	1.7	1.3	2.1	1.8	2.1	5.0
GPP (g C m <sup>-2</sup> year <sup>-1</sup> )																					~				
	284	237	197	434	299	581	570	241	275	319	312	774	598	772	952	712	737	989	975	1617	1048	1157	329	096	1017
TAVE (°C)	-10.6	-5.9	0.7	-0.4	-2.9	-0.2	-0.7	2.5	5.1	4.7	-1.5	10.0	9.5	8.3	11.0	4.9	7.0	11.3	10.9	15.1	15.5	15.5	15.0	13.7	13.7
DOM_VEG	aerenchymatous	aerenchymatous	aerenchymatous	aerenchymatous	moss_sphagnum	aerenchymatous	eri_shrub	moss_sphagnum	moss_sphagnum	moss_sphagnum	moss_sphagnum	aerenchymatous	aerenchymatous	tree	aerenchymatous	eri_shrub	aerenchymatous	aerenchymatous	aerenchymatous	aerenchymatous	aerenchymatous	aerenchymatous	aerenchymatous	aerenchymatous	aerenchymatous
Longitude	161.351	-149.311	19.0452	24.20918	-147.856	-148.313	-148.321	19.55654	24.1699	24.19293	-121.299	12.17611	12.88901	11.3275	2.284102	-89.9792	141.8107	-82.9962	127.2506	-121.647	-121.641	-121.765	-121.755	140.0269	175.554
Latitude	68.617	909.89	68.356	67.99724	64.86627	64.70373	64.69555	64.18203	61.83746	61.83256	61.308	54.21028	53.8759	47.80639	47.32291	46.0827	43.32301	41.46464	38.2013	38.107	38.103	38.05	38.037	36.054	-37.388
Wetland type	Tundra	Tundra	Bog	Fen	Bog	Fen	Bog	Fen	Bog	Fen	Bog	Fen	Fen	Bog	Fen	Fen	Bog	Marsh	Rice	Marsh	Marsh	Marsh	Marsh	Rice	Bog
Site	RU-Ch2	US-Ics	SE-Sto	FI-Lom	US-Uaf	US-Bzf	US-Bzb	SE-Deg	FI-Si2	FI-Sii	CA-SCB	DE-Hte	DE-Zrk	DE-Sfn	FR-LGt	US-Los	JP-Bby	US-Wpt	KR-Crk	US-Tw1	US-Tw4	US-Myb	US-Sne	JP-Mse	NZ-Kop

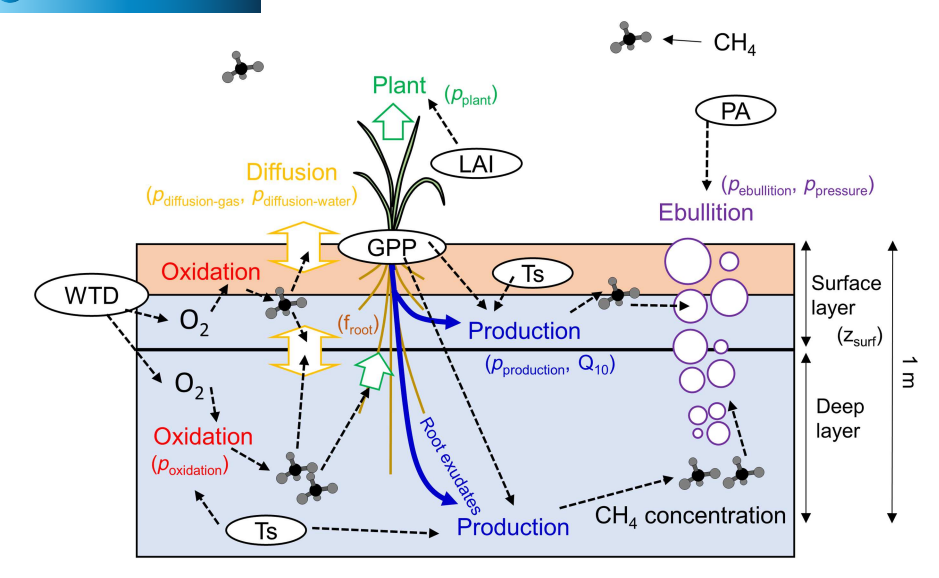


FIGURE 1 Schematic representation of the model structure for methane ( $\mathrm{CH_4}$ ) flux. The model consists of two soil layers: a surface layer susceptible to oxic conditions and a deep layer prone to anoxic conditions. Ecosystem-atmosphere  $\mathrm{CH_4}$  fluxes are the net result of  $\mathrm{CH_4}$  production ( $p_{\mathrm{production}}$  and  $Q_{10}$ ), oxidation ( $p_{\mathrm{oxidation}}$ ), and transport processes. Transport is the sum of diffusion ( $p_{\mathrm{diffusion-gas}}$  and  $p_{\mathrm{diffusion-water}}$ ), plant-mediated transport ( $p_{\mathrm{plant}}$ ), and ebullition ( $p_{\mathrm{ebullition}}$  and  $p_{\mathrm{pressure}}$ ). Substrate for  $\mathrm{CH_4}$  production associated with gross primary productivity (GPP) is divided into surface and deep layers ( $z_{\mathrm{surf}}$ ), considering root distribution ( $f_{\mathrm{root}}$ ). The model is driven by biophysical variables: soil temperature ( $T_{\mathrm{S}}$ ) in the two soil layers, water table depth (WTD), leaf area index (LAI), GPP, and barometric pressure (PA). Calibrated parameters are shown with parentheses, and dashed lines represent a major flow of causality.

used in current process-based models (Raivonen et al., 2017; Riley et al., 2011; Walter & Heimann, 2000; Wania et al., 2010). The simple formulation of iPEACE allows to effectively fit the model to data at reduced computational costs. The model is driven with GPP for substrate availability, LAI for transport potential through plant stems, soil temperature in the two layers for driving kinetics, oxygen  $(O_2)$  concentration for redox potential, WTD for diffusivity and hydrostatic pressure that drives ebullition, and PA for ebullitive transport. The  $O_2$  concentration was not included in the FLUXNET-CH $_4$  database, and thus was determined from WTD. When the water table position is above or below a soil layer, the layer is assumed to be anoxic or fully oxic, respectively. When WTD is within a soil layer,  $O_2$  concentration in that layer is linearly related to that fraction of the layer that is inundated between fully oxic to anoxic conditions.

To explore the underlying processes, the model contains 10 parameters and two initial values of the  $\mathrm{CH_4}$  pools in each soil layer (mol- $\mathrm{CH_4}$  m $^{-3}$ ), which are calibrated with data (Table 3). For adapting the model to the current analysis, the thickness of the surface layer and root fraction (described below) in the surface layer are calibrated for each site, whereas the previous study (Ueyama et al., 2022) used a fixed value.

Thickness of the surface layer ( $z_{\rm surf}$ ; m) is the parameter constrained by the data. Thickness of the deep layer is calculated as the difference between total soil thickness (1 m, except for permafrost sites) and the thickness of the surface layer. For sites affected by permafrost, total soil thickness is defined as the active layer depth (0.5 m for RU-Ch2, 1.0 m for US-ICs, and 0.6 m for US-Uaf). Seasonal changes in soil thickness associated with soil thaw are not considered in the model for simplicity. Surface root fraction (fs<sub>root</sub>) is the

parameter explaining how roots are concentrated in the surface layer relative to the total roots. The model assumes that root density is higher in the surface layer than the deep layer.

Methane production is assumed to depend on substrate availability from GPP, kinetics as determined by soil temperature, and anaerobic status as determined by O2 concentration. The fraction of GPP to  $CH_4$  substrate ( $p_{production}$ ; mmol- $CH_4$  g<sup>-1</sup> C) and temperature sensitivity  $(Q_{10})$  are both empirical parameters. Modeled  $CH_4$  production increases with soil temperature and substrate availability but decreases with increased  $O_2$  concentration. The  $p_{production}$  parameter is the aggregated parameter for explaining the fraction of root exudates from GPP and the efficiency from exudates to CH₄ production and relates to the base production rate in a  $Q_{10}$  equation (Chen, 2021). The model does not explicitly consider anaerobic peat decomposition; thus, CH<sub>4</sub> production by decomposition are implicitly incorporated through a decrease in the CH<sub>4</sub> pools. Partitioning of CH<sub>4</sub> substrate in each soil layer is assumed to be a function of the root distribution between the surface and deep soil layers. CH<sub>4</sub> oxidation is calculated with a Michaelis-Menten equation (Wania et al., 2010) with CH<sub>4</sub> concentration and O2 concentration, where the maximum CH4 oxidation rate ( $p_{oxidation}$ ; mol-CH<sub>4</sub> m<sup>-3</sup> s<sup>-1</sup>) is a calibrated parameter.

Plant-mediated transport is calculated by the concentration gradient between a soil layer and the atmosphere, root fraction in each layer, and LAI. The transfer efficiency under a given concentration gradient ( $p_{plant}$ ;  $10^{-3} \, day^{-1}$ ) is a calibrated parameter. The model does not consider CH<sub>4</sub> transport by dead plants, which are not accounted for by LAI, with the assumption that collapsed aerenchymatous tissue in senesced leaves has low transport capacity (Korrensalo et al., 2022).

TABLE 3 Ranges of parameters for mathematical optimization and prior distributions for Bayesian optimization for the iPEACE model. The range of uniform distributions were determined by adding plus/minus to the values determined by the differential evolution method for each site (Table S1).

Parameter	Unit	Lower range in mathematical optimization	Upper range in mathematical optimization	Prior range in Bayesian inference	Prior distribution
Initial CH <sub>4</sub> value at the surface layer	mol-CH <sub>4</sub> m <sup>-3</sup>	0	0.5	±0.1	Uniform
Initial CH <sub>4</sub> value at the deep layer	$mol-CH_4 m^{-3}$	0	4	±0.2	Uniform
Base production rate per gross primary productivity ( $p_{production}$ )	mmol-CH <sub>4</sub> g C <sup>-1</sup>	1	6	±0.5	Uniform
Temperature sensitivity of $\mathrm{CH_4}$ production $\mathrm{(Q_{10producton})}$	-	0.00001	5	±1	Uniform
Maximum $CH_4$ oxidation rate ( $p_{oxidation}$ )	$\mathrm{mol}\text{-}\mathrm{CH_4}\mathrm{m^{-2}}\mathrm{s^{-1}}$	0.000000125	0.000125	±log(1.0)	Uniform
Nondimensional conductivity for gaseous transfer ( $p_{\rm ebullition}$ )	-	0	0.01	b	Uniform
Diffusion coefficient for plant-mediated transport ( $p_{\rm plant}$ )	10 <sup>-3</sup> day <sup>-1</sup>	0.001	3	±1	Uniform
Diffusion coefficient multiplier for water $(p_{\text{diffusion-water}})$	-	0.001	2	±0.3	Uniform
Diffusion coefficient multiplier for gas $(p_{\text{diffusion-gas}})$	-	0.001	2	±0.3	Uniform
Sensitivity of ebullition to barometric pressure $(p_{pressure})$	hPa <sup>-1</sup>	0	1	±0.05	Uniform
Thickness of the surface layer $(z_{surf})$	m	0.05	0.80	0.05-0.80	Uniform
Surface root fraction (fs <sub>root</sub> )	-	0.05	1.00	0.05-1.00	Uniform
Residuals of the model	$\mathrm{mg}~\mathrm{CH_4}~\mathrm{m^{-2}}~\mathrm{day^{-1}}$	-	-	-	Log normal

Ebullitive transport is calculated based on a concentration threshold scheme (Peltola et al., 2018), which has two empirical parameters: nondimensional conductivity for bubble transport  $(p_{\text{ebullition}})$  and a parameter for explaining episodic  $CH_{\Delta}$  bubble transport driven by barometric pressure changes ( $p_{pressure}$ ; hPa<sup>-1</sup>). Since the model assumes that CH<sub>4</sub> is not immediately emitted as ebullition but accumulated as bubbles, p<sub>ebullition</sub> represents the transport efficiency of bubbles. The p<sub>pressure</sub> parameter empirically explains the sensitivity to decreasing barometric pressure, i.e., the relative increase in ebullition per 1 hPa decrease in mean PA. In the model, the ebullition flux from each layer is assumed to be directly transported to the atmosphere, when WTD is within the top 10 cm of the soil based on a field study (Stanley et al., 2019). When WTD is deeper than 10 cm, CH<sub>4</sub> transport through ebullition is added to the surface layer CH<sub>4</sub> pool, which is a modification from the original model of Ueyama et al. (2022).

Diffusive flux is calculated using Fick's first law. The diffusion coefficients for gas and water are calculated based on Riley et al. (2011), and then their calibrated correction factors ( $p_{\rm diffusion-gas}$  and  $p_{\rm diffusion-water}$ ) are multiplied to the respective diffusion coefficients.

## 2.3 | Model applications

The model parameters, initial conditions, and model error  $(\sigma)$  were determined from the observed data by the Bayesian method as follows:

$$F_{\text{OBS}} \sim \text{Normal}(F_{\text{MODEL}}, \sigma^2)$$
 (2)

where the function *Normal* represents the normal distribution,  $F_{\rm OBS}$  is the observed CH<sub>4</sub> emission, and  $F_{\rm MODEL}$  is the modeled CH<sub>4</sub> emission. The a priori distribution of  $\sigma$  was assumed to be a log normal distribution with mean of log(0.5) mg CH<sub>4</sub> m<sup>-2</sup> day<sup>-1</sup> and standard deviation of 0.1 mg CH<sub>4</sub> m<sup>-2</sup> day<sup>-1</sup>, where the hierarchical structure was used to reduce computational costs. Equation 2 assumes that variance for the model-observation mismatch was temporally uniform without incorporating temporal correlation in the observed data.

The a priori distributions of the parameters were generally assumed to be uniform (Table 3). The range of uniform distributions were determined by adding plus/minus to the values determined by the differential evolution method for each site (Table S1). The preconstraint of a priori distribution effectively reduces computational costs without decreasing model performance and improves model convergence, based on a preliminary analysis. For constraining the behavior that root density must be higher in the surface layer than the deep layer in the Bayesian optimization, the thickness of the surface layer and root distribution were determined without results from the mathematical optimization. For the parameter optimization, we did not assume the hierarchy in the statistical model.

The posterior distributions of the parameters were estimated using a Markov Chain Monte Carlo (MCMC) method with the No-U-Turn Sampler (NUTS). NUTS is an extension of Hamiltonian Monte Carlo and provides very effective samples without requiring user intervention or costly tuning runs (Hoffman & Gelman, 2014). The

efficiency of NUTS was more than 1000 times that of Metropolis or Gibbs sampling. Posterior distributions of the parameters were estimated using four chains with 1000 samples after warm-up based on 1000 sampling. Bayesian inference was performed using the PyStan library (version 2.19.1.1). Owing to a complex and multimodal parameter space, consistent solutions from each chain were not obtained or some chains were not converged for some sites. In this case, we used results from chains that estimated the lowest model errors. The conservative treatment was required because bad chains seem to converge to local minima rather than to mathematically meaningful multimodal distributions and the problem was not fixed using different a priori, different initial values or further sampling. The trace plots and probability density functions for all parameters in all sites are shown in Figure S1, which shows that at least two chains were well converged. Convergence of MCMC was evaluated by the Gelman-Rubin method with the potential scale reduction factor (PSRF), which showed that all parameters for all sites were well converged (PSRF <1.05) except slightly high PSRF for two parameters for US-Uaf (PSRF <1.12; Table S3). Computational costs of the Bayesian inference ranged from 0.35 h to 2.5 days per site with an average of 6.16 h (Table S4).

Model parameters were estimated using daily CH<sub>4</sub> fluxes and the ancillary biophysical variables. Specifically, we used daily gap-filled CH<sub>4</sub> flux (FCH4\_F), which contained only long data gaps (>2 months), and did not assume embedded functional relationships. In addition, we used FCH4\_F\_ANN\_median when uncertainties in the neural network (FCH4\_uncertainty) were less than absolute of FCH4\_F\_ ANN median. The use of gap-filled fluxes with low uncertainties could prevent propagating uncertainties associated with long-term gap-filling data into the parameter estimation. We also evaluated how the gap-filled data influenced modeled processes, where we eliminated data records where daily CH<sub>4</sub> emission contained more than 80% gaps in half-hourly data, in constraining the model. Apart from this issue, some high-latitude and rice paddy sites provided only growing-season fluxes, which hampered constraining the model for cold non-growing and fallow seasons, respectively. We also found that flux data for the first few days of a model run were important for constraining the initial CH<sub>4</sub> pools (i.e., initial conditions). Without the data, initial conditions were not well converged, and estimated dormant season emissions were unrealistic. Consequently, when FCH4\_F was missing, we used the gap-filled CH4 flux (FCH4\_F\_ ANN\_median) during the first days of a model run and for the winter period (air temperature < -10°C). The benefits of selectively using gap-filled data could outweigh the propagation of gap-filled errors, where unrealistic CH<sub>4</sub> emissions were not estimated.

The model constraints for each site were evaluated by RMSE normalized by mean, R, and normalized standard deviation (SD) in daily CH<sub>4</sub> flux. For further interpreting and analyzing modeled results, we eliminated unconstrained site-data where normalized RMSE was >0.9, R was <0.6, normalized SD was <0.7, or normalized SD was >1.3.

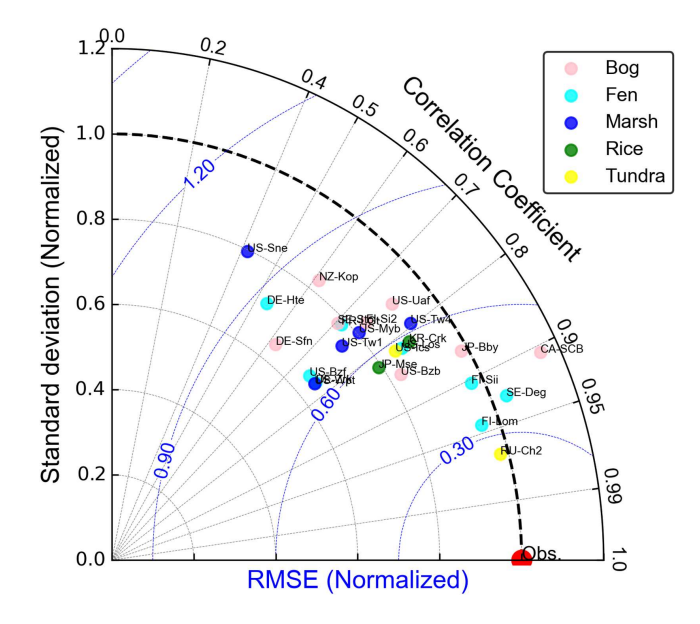
The sensitivities to the forcing variables were performed using the models successfully constrained for each site. First, we applied perturbations to the inputs of: (1) 1°C increase to the observed soil temperatures, (2) 10% increase in GPP and LAI, (3) 10 cm increase in WTD, and (4) 10 cm decrease in WTD with all other inputs held at measured conditions. Next, we examined the changes in modeled  $CH_4$  emissions with unperturbed input (control experiment). We conducted the sensitivity analysis for sites spanning at least 3 years of data because the uncertainties are high in models constrained by short-term data (Ueyama et al., 2022).

To understand the variabilities in the estimated parameters across the sites, we applied principal component analysis (PCA) toward seven parameters:  $p_{\rm production}$ ,  $Q_{\rm 10production}$ ,  $p_{\rm oxidation}$ ,  $p_{\rm ebullition}$ ,  $p_{\rm plant}$ ,  $p_{\rm diffusion-water}$ , and  $p_{\rm pressure}$ . The parameter for gas diffusion ( $p_{\rm diffusion-gas}$ ) was not included in the PCA because  $p_{\rm diffusion-gas}$  did not show a bell-shaped density curve at approximately half of the sites (Figure S1). The parameters were first standardized with mean and SD and then compressed into two principal components (PC) using the scikit-learn library in python. We chose two principal components because they explained more than 70% of the variance in the parameters across the sites.

#### 3 | RESULTS

# 3.1 | Model performance

Across the 25 sites, 19 sites had reliable performance that satisfied the criterion for normalized RMSE, R, and normalized SD (section 2.3). According to the Taylor diagram (Figure 2), model-data agreement was the best (R > 0.9) for RU-Ch2, FI-Lom, SE-Deg, FI-Sii, and CA-SCB. Among the accepted 19 sites, the median of normalized RMSE, R, and normalized SD were 0.59, 0.82, and 0.87, respectively.



<code>FIGURE 2 Taylor</code> diagram of the model performances in daily methane ( $CH_4$ ) fluxes for each site. The benchmark corresponding to observations is shown as Obs with red dots. RMSE, root mean square error.

Except for the five sites with good model fit noted above, the model underestimated the SD of CH<sub>4</sub> flux, where the mean and SD of the normalized SD was 0.84±0.13 across all sites. For the six sites excluded from subsequent analyses due to low performance (US-Sne, DE-Hte, DE-Zrk, DE-Sfn, US-Bzf, and US-Wpt), the mean seasonality was inconsistent between observations and models (Figure 3), despite a moderate R and normalized RMSE. The low performance may represent a lack of important processes in the model and insufficient data to constrain the model. For example, US-Sne is a newly restored wetland and has a heterogeneous surface of open water and emergent vegetation, which make it difficult to constrain the processes based only on measured CH<sub>4</sub> fluxes for 3 years. Overall, there was no significant difference in the model performance in terms of wetland type and the number of years used for calibration.

In general, there were no obvious differences in modeled results with the optimized data containing fully gap-filled data or data when excluding days with >80% gaps. However, five sites (US-Sne, DE-Hte, DE-Zrk, FR-LGt, and NZ-Kop) did not meet the standard for a well constrained model with the non-gap-filled data (Figure S2). The median of normalized RMSE, R, and normalized SD were 0.57, 0.83, and 0.90, respectively, in the model with the data not containing fully gap-filled data. The estimated CH<sub>4</sub> transport, production, and

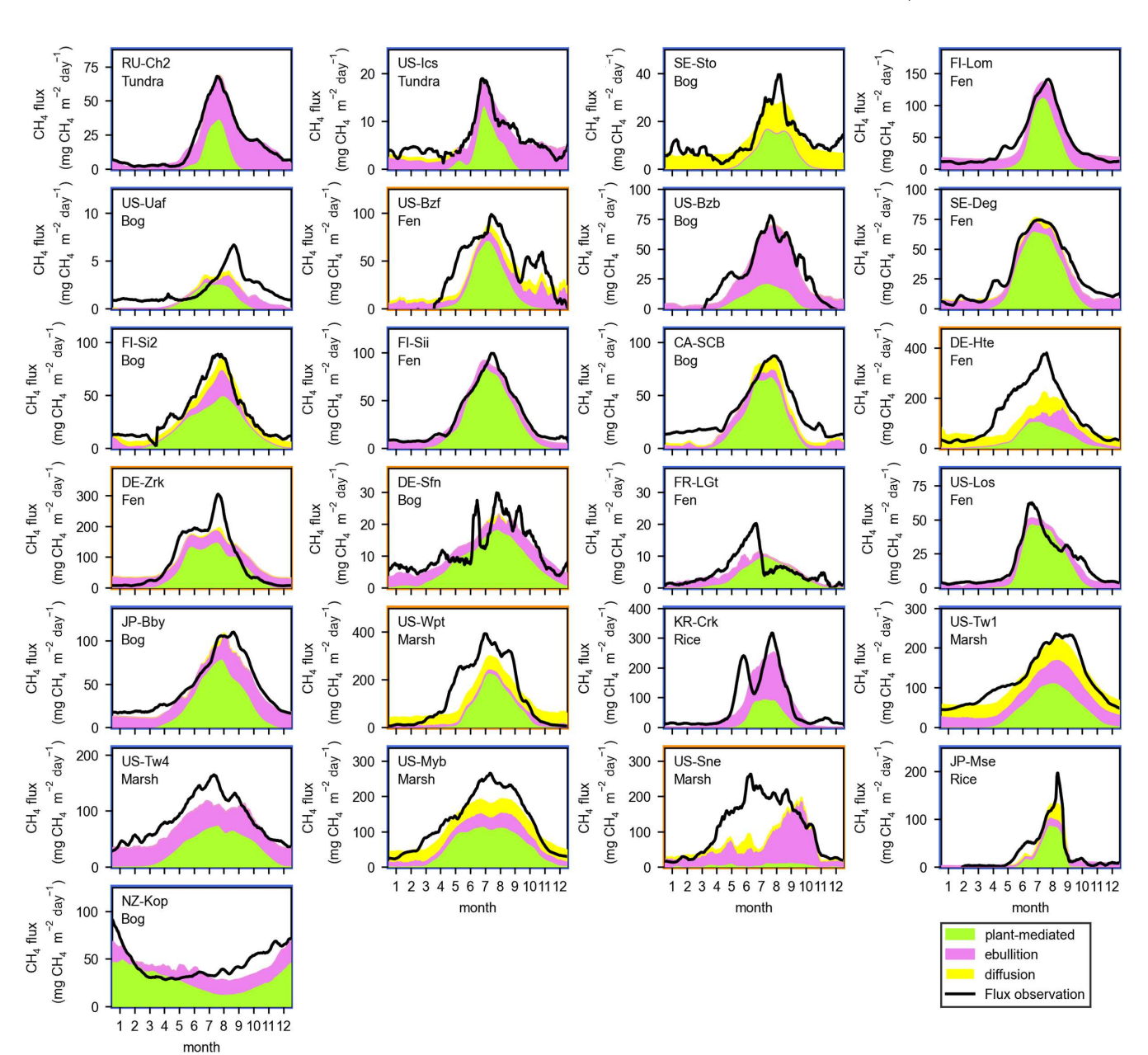


FIGURE 3 Mean seasonal variations of observed and modeled methane (CH<sub>4</sub>) fluxes and the transport components of plant-mediated transport, ebullition, and diffusion. The seasonality is calculated as a mean across years, and then a seven-day moving mean is applied for smoothing. Note differences in y-axis ranges among panels. Frames colored by blue are the sites having acceptable model performance (normalized root mean square error was >0.9, correlation coefficient was <0.6, normalized standard deviation was <0.7, or normalized standard deviation was >1.3), and those colored by brown are the sites having low performance.

oxidation were also consistent among the two models constrained with two data criteria, except for sites having low record numbers (e.g., RU-Ch2 and JP-Mse) (Figure S3). Other results, including intersite differences in  $\mathrm{CH_4}$  emission processes and sensitivity to biophysical drivers, were generally consistent among the two models constrained with two data criteria.

## 3.2 | Estimated transport processes

Based on model results, plant-mediated transport and ebullition were more important pathways for CH<sub>4</sub> emissions than diffusive transport across sites (Figures 3 and 4; Table 2). In most cases, plant-mediated transport tended to be the major pathway for fen sites  $(72\% \pm 10\%, n = 8; \text{mean} \pm SD)$  and bog sites  $(55\% \pm 16\%, n = 8;$ mean  $\pm$  SD) (Figure 4). Ebullition accounted for 27%  $\pm$  10% of the total emission for the fen sites and  $26\% \pm 10\%$  for the bog sites. In contrast, ebullition was estimated to be the major pathway at the two tundra sites (64% ± 4%) owing to shallow WTD (Figure 4). Because the modeled plant-mediated transport increased with LAI, relative contribution of ebullition and/or diffusion was found high during periods of low LAI. When LAI was ≥20% of the annual peak, plantmediated transport was the major pathway (70% ± 14%), except for three sites (RU-Ch2, US-Bzb, and KR-Crk) during the growing season (Figure 3; Table 2). Diffusion was a minor pathway at most sites, but tended to be high in two marsh sites (US-Myb and US-Tw1) and a bog site (SE-Sto). For the three sites, the model predicted an anoxic surface layer, negligible oxidation, and high CH<sub>4</sub> concentrations in the surface layer at high WTD sites, allowing for surface diffusion. Since US-Myb was a restored wetland, the contribution of diffusion was approximately half of the CH4 emissions in open water conditions

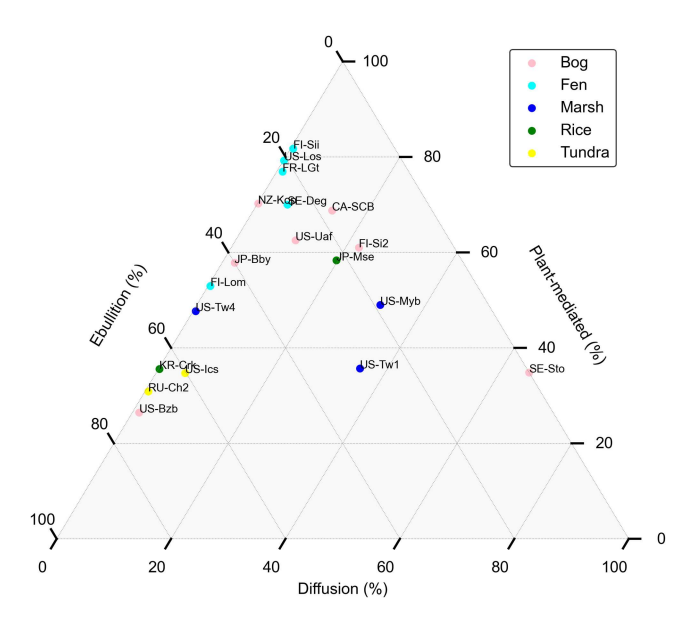


FIGURE 4 Ternary plot for modeled annual methane (CH<sub>4</sub>) transport pathways of plant-mediated transport, ebullition, and diffusion.

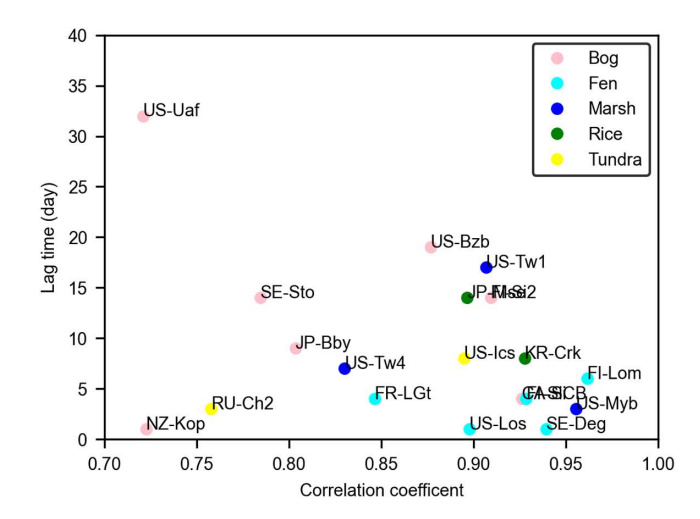


FIGURE 5 Lag time between modeled methane ( $CH_4$ ) production and  $CH_4$  flux based on a cross-correlation analysis, plotted against the correlation coefficient between  $CH_4$  fluxes and lagged  $CH_4$  production.

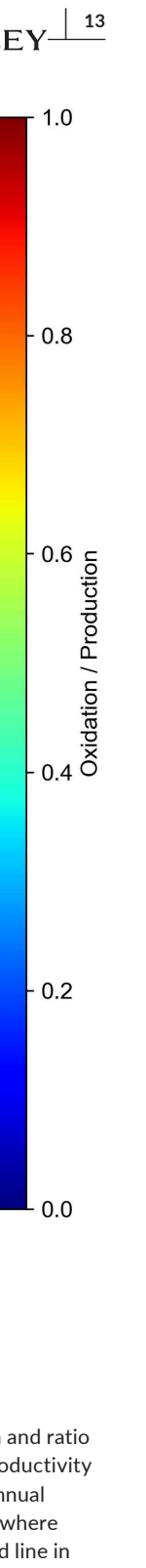
(2010–2011) and then decreased to  $31\% \pm 6\%$  with the expansion of emergent vegetation from 2012 to 2018.

Based on cross-correlation analysis,  $CH_4$  emissions lagged  $CH_4$  production by 1–32 days (Figure 5). There was more than a 30-day lag between  $CH_4$  production and  $CH_4$  emissions at US-Uaf. Lags tended to be, on average, longer in bogs ( $13\pm10\,\mathrm{days}$ ; n=7; mean $\pm SD$ ) than in fens ( $3\pm2\,\mathrm{days}$ ; n=5), rice paddies ( $11\pm3\,\mathrm{days}$ ; n=2), or tundra ( $6\pm3\,\mathrm{days}$ ; n=2). Even in a long-lagged site (> 30 days for US-Uaf), the correlation between  $CH_4$  production and  $CH_4$  emission was good (R>0.70), indicating that  $CH_4$  production controlled temporal variations in  $CH_4$  emission.

Inter-site variations in CH<sub>4</sub> production explained inter-site variations in CH<sub>4</sub> emissions ( $R^2 = 0.72$ ; p = .01), except for sites where the ratio of oxidation to production was high (Figure 6a). For sites with high oxidative fraction to production, CH<sub>4</sub> emissions were relatively low considering their production (Figure 6a). These sites with high oxidation generally exhibited low minimum WTD (Figure 6b). CH<sub>4</sub> production and emission were positively correlated with soil temperature and GPP across the sites having low oxidation (Figure 6c-f). This result is unexpected because the model was constrained in each site using temporal variations in the variables, as there was no assumption about inter-site variations in constraining the model. Based on the variable importance analysis using random forest regression, soil temperature and GPP almost equally explained the inter-site variations in CH<sub>4</sub> production. In contrast to production and oxidation, inter-site variations in three transport pathways did not correlate with CH₁ emissions.

## 3.3 | Estimated parameters

Most parameters in our model were well converged (Table S3), but  $p_{\rm diffusion\text{-}gas}$  did not show a bell-shaped density curve with a single peak at 8 of the 19 sites (Figure S1). Substrates for CH<sub>4</sub> production



3652486, 0, Downloaded from https://onlinelibrary.wiley.com/doi/10.1111/gcb.16594 by University Of Alaska Fairbanks, Wiley Online Library on [20/01/2023]. See the Terms

Wiley Online Library for rules of use; OA articles are governed by the applicable Creative Commons License

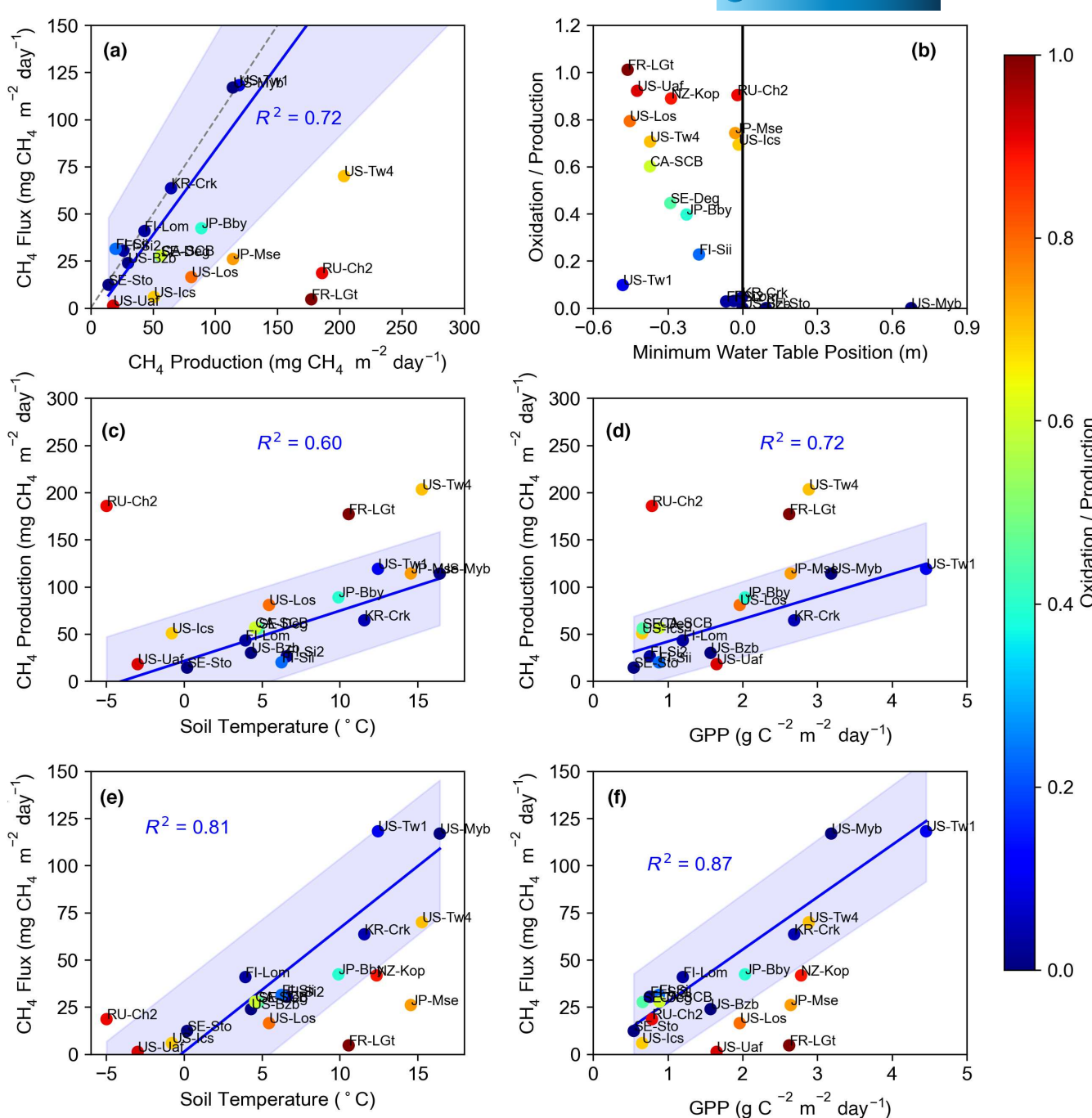


FIGURE 6 Relationships between modeled methane (CH<sub>4</sub>) production and CH<sub>4</sub> flux (a), between minimum water table position and ratio of oxidation to production (b), between mean annual soil temperature and modeled CH<sub>4</sub> production (c), between gross primary productivity (GPP) and modeled  $CH_4$  production (d), between soil temperature and modeled  $CH_4$  flux (e), and between GPP and  $CH_4$  flux (f). Annual mean or minimum for the study period are shown. Blue lines in (a, c, d, e, f) represent linear regression (all p < .001) based on sites where modeled oxidation contributed less than 70% of  $CH_4$  production, where shading represents the prediction interval (p = .1). Dashed line in (a) represents the 1:1 line between production and flux. The high  $CH_4$  production for NZ-Kop (525 mg  $CH_4$  m<sup>-2</sup> day<sup>-1</sup>) is too high to fit the range in the figure (a, c, d). Points represent mean values over the observation period, and their colors represent the ratio of CH<sub>4</sub> oxidation to production.

per GPP ( $p_{production}$ ) were converged on the lower end of a priori range (median =  $1.1 \,\mathrm{mmol}\,\mathrm{m}^{-2}\,\mathrm{g}\,\mathrm{C}^{-1}\,\mathrm{m}^2$ ) over the 19 sites. The median and SD of  $Q_{10}$  of  $CH_4$  production was  $3.7 \pm 1.9$ , where there was a weak negative correlation between  $p_{\rm production}$  and  $Q_{10}$  across the sites ( $R^2 = 0.31$ ; p = .01). The maximum oxidation parameter was

estimated to be in the middle of the prescribed upper and lower range at most sites. Estimated  $\mathbf{p}_{\text{ebullition}}$  and  $\mathbf{p}_{\text{plant}}$  were not correlated with contributions from ebullition and plant-mediated transport to CH<sub>4</sub> emission, respectively. Ebullition from 9 sites had a marginal sensitivity to pressure decline (<2% hPa<sup>-1</sup>), where there was no

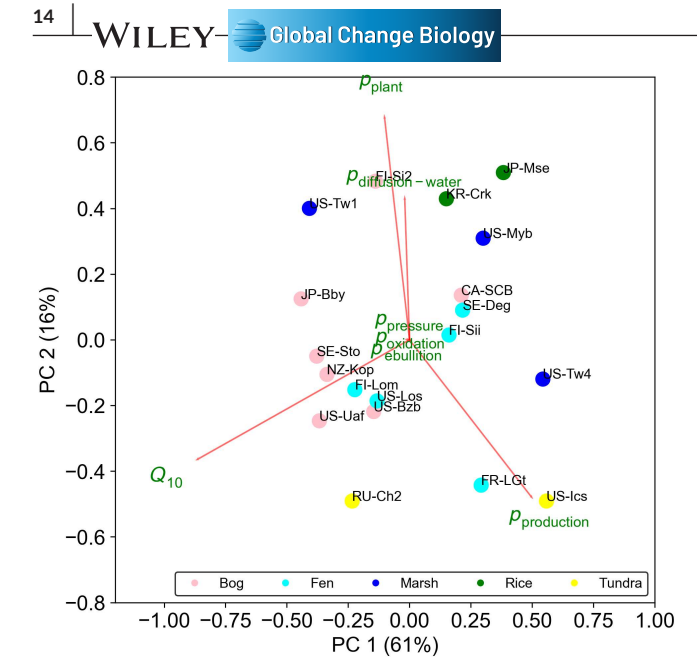


FIGURE 7 Biplots showing the first and second components based on the principal components (PC) of the estimated parameters across the sites: methane (CH<sub>4</sub>) production per gross primary productivity ( $p_{\text{production}}$ ),  $Q_{10}$  for CH<sub>4</sub> production, maximum CH<sub>4</sub> oxidation rate ( $p_{\text{oxidation}}$ ), nondimensional conductivity for gaseous transfer ( $p_{\text{ebullition}}$ ), diffusion coefficient for plantmediated transport ( $p_{\text{plant}}$ ), diffusion coefficient multiplier for water ( $p_{\text{diffusion-water}}$ ), and sensitivity of ebullition to barometric pressure ( $p_{\text{pressure}}$ ).

correlation between  $p_{pressure}$  and contributions of ebullition to the total emission across the sites. There was no significant difference (p < .05) in all parameters aggregated by aerenchymatous and moss vegetation.

Based on the PCA analysis, 77% of the variance in the parameters among the sites was compressed with two PCs (Figure 7). The first PC represented a tradeoff of two parameters for  $\mathrm{CH_4}$  production between high  $p_{\mathrm{production}}$  and low  $Q_{10}$  and vice versa, representing 61% of the parameter distribution across the sites. The second PC explained 16% of the distribution and represented a tradeoff between  $\mathrm{CH_4}$  production and transport through plants and gas diffusion. There were weak clusters for bog sites with relatively high  $Q_{10}$ , tundra sites with low transport parameters, and rice paddies with high transport parameters. No clusters were apparent for fen and marsh sites.

The thickness of the surface layer,  $z_{\rm surf}$ , was the conceptual depth separating surface oxic and deeper anoxic layers, and thus negatively correlated to WTD for sites where minimum WTD was below  $-0.1~{\rm m}$  ( $z_{\rm surf}=-1.2~{\rm WTD}-0.05~{\rm m}$ ;  $R^2=0.48$ ; p=.03; n=10). The regression analysis showed that  $z_{\rm surf}$  was close to minimum WTD. In contrast, there was no significant trend in the surface layer thickness for sites with high mean annual WTD (> $-0.1~{\rm m}$ ). For sites with high WTD (i.e., always above the ground surface), the thickness of the soil layers did not control the degree of redox conditions for the two layers because the surface layer was always anaerobic.

# 3.4 | Sensitivity to biophysical variables

Based on the sensitivity analysis,  $CH_4$  emissions increased by 9.6% or 3.5 g  $CH_4$  m<sup>-2</sup> year<sup>-1</sup> (median relative increase), with 10% increase in GPP across the sites, with the increases higher in the sites with high annual soil temperatures (Figure 8a). The sensitivity analysis was performed on sites that had at least 3 years of data (14 sites) among the 19 sites. The sensitivities aggregated for high or low WTD sites (sites having mean water table position above or below the ground surface) indicated that the relative increases in  $CH_4$  emissions did not differ significantly between the two WTD classes (p=.35 in Welch's t test; inset in Figure 8a).

The 1°C increases in soil temperatures increased  $CH_4$  emissions by 6.6% or 2.5 g $CH_4$  m $^{-2}$  year $^{-1}$  (median relative increase) (Figure 8b). The increases were similar in magnitude to those from the 10% increase in GPP. Compared with the sensitivity to GPP, the increased magnitudes appeared to not be clearly related to the mean annual soil temperatures and WTD, likely because temperature sensitivity ( $Q_{10}$ ) for  $CH_4$  production differed by site. The increases in  $CH_4$  emissions also did not differ significantly between the two WTD classes (p=.80; inset in Figure 8b).

The increase in CH<sub>4</sub> emissions with 1°C increases were lower than those estimated based on an empirical  $Q_{10}$  relationship between daily mean soil temperature and CH<sub>4</sub> emissions (Figure 9). Eight of the 14 sites were estimated to have higher CH<sub>4</sub> emission sensitivity using the empirical  $Q_{10}$  model than iPEACE. Across all 14 sites, the relative increases in CH<sub>4</sub> emissions tended to be higher in the empirical  $Q_{10}$  model (12%) than the iPEACE model (8%) across the sites (p=.12) (US-Uaf was not included in relative changes in emission owing to the small magnitude in emission).

Decreased  $CH_4$  emissions associated with a 10 cm decrease in WTD were greater than increased  $CH_4$  emissions with a 10 cm increase in WTD (Figure 8c,d). A decrease in WTD decreased  $CH_4$  emissions at most sites and vice versa, where the median changes by the decrease and increase in WTD were – 31% and + 6.5%, respectively. A site with a WTD permanently well above the ground surface (US-Myb) did not exhibit significant responses to changing WTD, as WTD always remained above the surface. The relative changes in  $CH_4$  emissions did not differ significantly between sites with low and high WTD with 10 cm increases in WTD (inset in Figure 8c; p = .34) and 10 cm decrease in WTD (inset in Figure 8d; p = .15).

There were two mechanisms for reduced  $\mathrm{CH_4}$  emissions by decreased WTD. The first mechanism is associated with changes in the frequency with which the surface layer becomes oxic conditions. In this mechanism,  $\mathrm{CH_4}$  production from the surface layer decreases when the WTD decreases with the perturbed input mostly fluctuating within the surface layer throughout the year. The second mechanism is related to the long-lasting change in redox conditions in the deep layer. We argue that reduced anaerobic conditions in the deep layer, which was rarely affected by oxic conditions with the unperturbed WTD, but was affected by the perturbed decrease in WTD. Owing to the loss of anaerobic conditions,  $\mathrm{CH_4}$  in the deep layer was consumed through oxidation; thus, the effects were relatively

3652486, 0, Downloaded from https://online/library.wiley.com/doi/10.1111/gcb.16594 by University Of Alaska Fairbanks, Wiley Online Library on [20/01/2023]. See the Terms and Conditions

on Wiley Online Library for rules of use; OA articles are governed by the applicable Creative Commons License

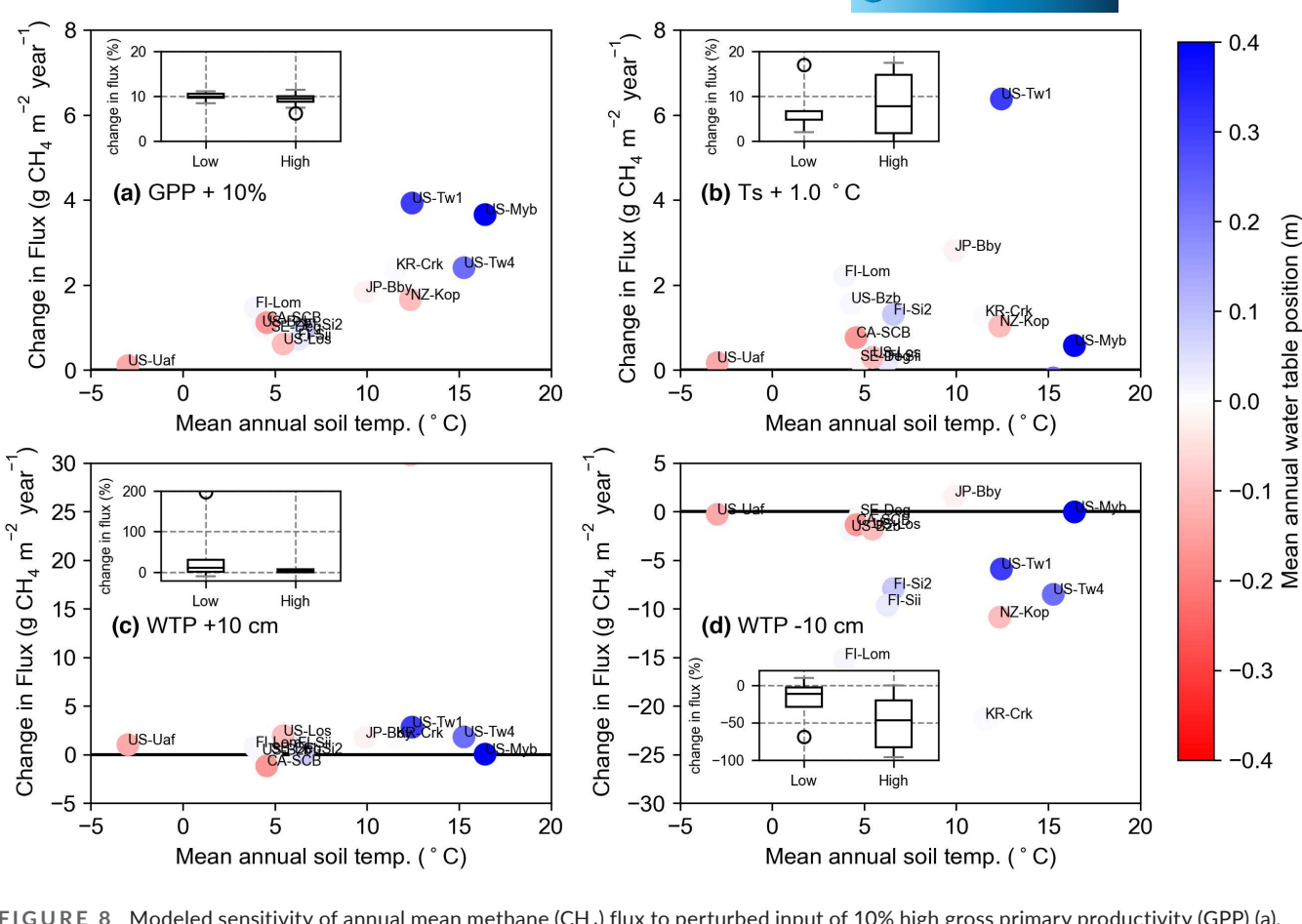


FIGURE 8 Modeled sensitivity of annual mean methane ( $CH_4$ ) flux to perturbed input of 10% high gross primary productivity (GPP) (a), biased input of 1°C high soil temperatures (Ts) (b), 10 cm high water table position (WTP) (c), and 10 cm low WTP (d). The changes in fluxes were shown on climate space of mean annual soil temperature and mean annual WTP over the observation period for each site. Boxplots represent the relative changes in flux for aggregated sites having annual high and low mean WTP (higher and lower above the ground, respectively), where dots represent outliers. The relative changes by boxplots did not include US-Uaf, because the flux was too low and the ratio was anomalously high due to low denominator. The sensitivity analysis was done for sites having at least 3 years of data.

long-lasting until  $CH_4$  concentrations built-up again. The median decrease in  $CH_4$  production was  $-6.9~\rm gCH_4~m^{-2}~\rm year^{-1}$ , and median increase in  $CH_4$  oxidation was  $12.9~\rm gCH_4~m^{-2}~\rm year^{-1}$ , indicating that the second mechanism was the major process responsible for the reduction in  $CH_4$  emissions. As an exceptional response examined at NZ-Kop, the decreased WTD could change sustained anoxic conditions to oxic conditions in the deep layer, resulting in decreased  $CH_4$  production, reduced  $CH_4$  pool, and finally decreased oxidation.

# 4 | DISCUSSION

The estimated processes for  $\mathrm{CH_4}$  emissions provide meaningful insights for interpreting observed data and estimating sensitivities to the forcing variables. The current analysis aims to shed light on the relative importance of processes involved in  $\mathrm{CH_4}$  production, transport, and oxidation across 25 freshwater wetland sites in temperate, boreal, and Arctic regions. The observed data included in the FLUXNET- $\mathrm{CH_4}$  database were used to constrain a process-based model which has a similar structure used in previous modeling studies (Riley et al., 2011; Walter & Heimann, 2000; Wania et al., 2010).

Flux partitioning is typically applied to net  $\mathrm{CO}_2$  fluxes for estimating GPP and ecosystem respiration (Reichstein et al., 2005), and has successfully provided deeper insights on their biotic and abiotic controls (Jung et al., 2017; Mahecha et al., 2010). Compared to the partitioning of  $\mathrm{CO}_2$  fluxes, more complex models are required to explain wetland  $\mathrm{CH}_4$  emissions and partition net  $\mathrm{CH}_4$  flux observations (Chen, 2021; Grant et al., 2019; Riley et al., 2011; Wania et al., 2010). Partitioned  $\mathrm{CH}_4$  fluxes can be useful for evaluating inter-site differences in fluxes (Figures 3 and 4), time lags between surface emissions and production (Figure 5), different responses of  $\mathrm{CH}_4$  processes (e.g., production, oxidation, and transport) to biophysical variables (Figures 6 and 8), and model parameterizations (Figure 7). Key processes and parameters estimated in this study need to be better constrained with further long-term observations and different data streams.

## 4.1 | Inter-site variations in estimated processes

The inter-site variations in CH<sub>4</sub> emissions were found to be primarily associated with those in CH<sub>4</sub> production rather than those in oxidation and transport (Figure 6), especially for sites with high WTD

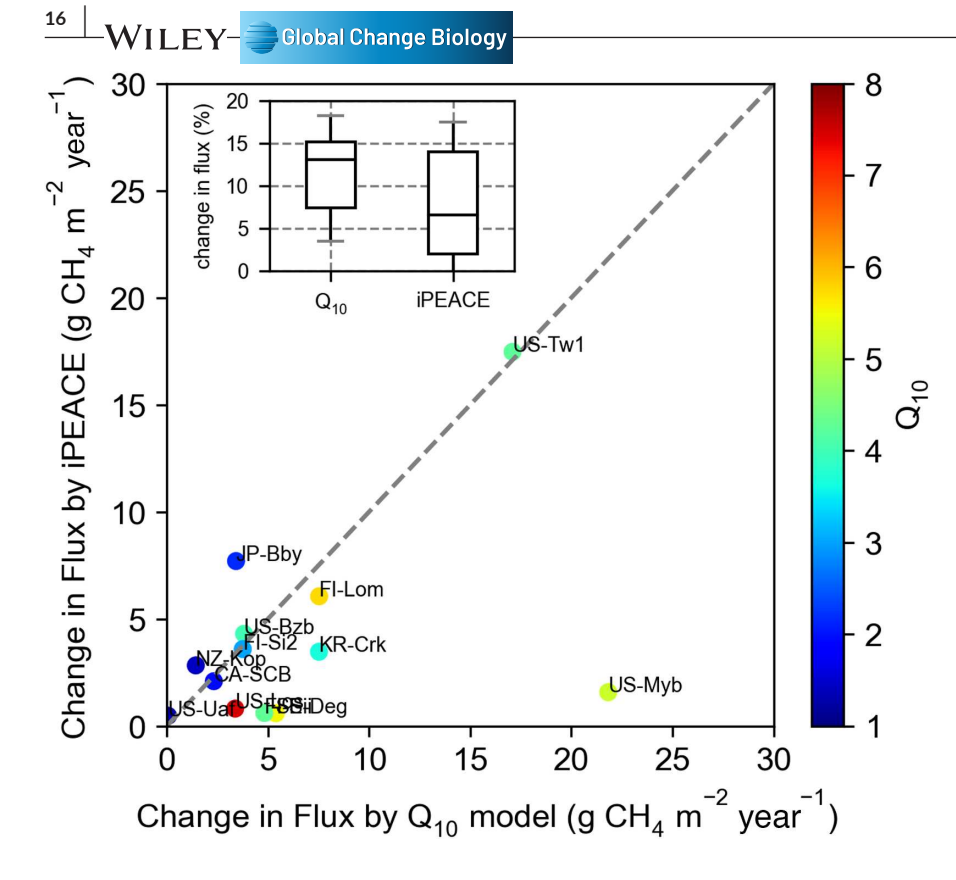


FIGURE 9 Change in methane ( $\mathrm{CH_4}$ ) flux estimated with a perturbed input of 1°C increase in soil temperatures for the empirical  $Q_{10}$  model and iPEACE model. The colors in plots represent the empirical  $Q_{10}$  value between daily  $\mathrm{CH_4}$  flux and soil temperature for the surface layer. Boxplots represent the relative changes in flux for aggregated sites having annual high and low mean water table positions (higher and lower above the ground, respectively). The relative changes by boxplots did not include US-Uaf, because the flux was too low and the ratio was anomalously high due to low denominator.

and low  $CH_4$  oxidation. These results could explain the correlation of annual  $CH_4$  emissions with mean annual air or soil temperature across global wetlands in the  $FLUXNET-CH_4$  database (Delwiche et al., 2021; Knox et al., 2019), where temperature was found to be an important driver of methanogenesis substrates (Chang et al., 2021) and  $CH_4$  production (Yvon-Durocher et al., 2014). In contrast, oxidation increased with decreasing WTD (Figure 6b), resulting in oxidation as the second most important process for explaining inter-site variations in  $CH_4$  emissions. These results are also consistent with global syntheses, which showed that a positive correlation between  $CH_4$  emissions and WTD was only detected in sites with relatively low WTD (i.e., mean annual WTD was below the soil surface) (Knox et al., 2019, 2021).

Transport processes were estimated to regulate the time-lag between  $\mathrm{CH_4}$  production and emissions (Figure 5), albeit we found no significant effect on total  $\mathrm{CH_4}$  emissions because annual emissions were mainly controlled by  $\mathrm{CH_4}$  production (Figure 6). The lag between production and emission occurred due to the time required to increase the  $\mathrm{CH_4}$  concentrations to drive  $\mathrm{CH_4}$  transport. The lag of  $\mathrm{CH_4}$  emissions to soil temperature or GPP was reported in studies using FLUXNET- $\mathrm{CH_4}$  (Chang et al., 2020; Delwiche et al., 2021; Knox et al., 2021; Yuan et al., 2022). For example, Knox et al. (2021) estimated that on average  $\mathrm{CH_4}$  emissions lagged soil temperature and GPP by 5.4days and 20.7 days, respectively, across wetlands globally. The lag between  $\mathrm{CH_4}$  emission and production (Figure 5) nonetheless partly explained the lag between emission and biophysical variables, as time is required for building up sufficient  $\mathrm{CH_4}$  concentrations driving  $\mathrm{CH_4}$  emissions.

# 4.2 | Sensitivities of CH<sub>4</sub> emissions to biophysical drivers

The estimated sensitivity of CH<sub>4</sub> emissions to GPP (Figure 8a, b) indicates the importance of substrate availability. A strong relationship between net ecosystem production and CH<sub>4</sub> emissions was previously reported across wetlands extending from subarctic peatlands to subtropical marshes associated with substrate availability (Whiting & Chanton, 1993). The estimated sensitivity occurred because CH<sub>4</sub> production in iPEACE was driven by GPP and soil temperature, reflecting the concept that increased GPP will increase substrate availability and thereby CH₄ emissions. The strong relationship with GPP (Figure 8a) was unexpected, however, because the sensitivity to GPP ( $p_{\rm production}$ ) was calibrated in each site and thus was expected to show high variability among the sites. It is worth noting that the estimated sensitivity to GPP might be caused by model assumptions. The model assumed that substrates for CH<sub>4</sub> were only provided by GPP but old peat previously fixed is also known to be a substrate for CH<sub>4</sub> production (Chasar et al., 2000). Substrates from recent primary production and peat organic carbon should be incorporated into future modeling with iPEACE.

Based on our sensitivity analyses,  $CH_4$  emissions were sensitive to a decrease in WTD for most sites (Figure 8). The most important mechanism associated with decreased WTD was increased oxidation at the deep layer. Because the buildup of the  $CH_4$  pool after loss of anaerobic conditions is time consuming, the effects can be long-lasting. This result is consistent with previous studies. Brown et al. (2014) indicated that a long recovery time was required for

CH<sub>4</sub> emissions after re-wetting following a drop in WTD at a site where the mean WTD was below the surface. They proposed a reason for the long recovery time as breaking the critical zone for CH<sub>4</sub> emissions by low WTD conditions. Simultaneously, when increased WTD resulted in aerobic layers switching to anaerobic conditions, CH<sub>4</sub> emissions increased, but the response was smaller than those to a decreasing WTD. This difference occurs because increased WTD increased the frequency of anoxic conditions at the surface layer, but the surface layer was still susceptible to oxic conditions even with perturbation increase in WTD, resulting in limited increases in CH<sub>4</sub> concentration. When deep soil remained anaerobic owing to shallow WTD, increases in soil temperature and GPP were equally important drivers of CH<sub>4</sub> emissions through kinetics and substrate availability, respectively (Figure 8).

# Comparison of estimated processes to observations from previous studies

Estimated transport flux was compared to EC measurements at various sites (Table 1). The high ebullition (50% of total emissions) was measured with chamber measurements at JP-Bby (Tokida, Miyazaki, et al., 2007, Tokida, Mizoguchi, et al., 2007), which was consistent with the current study. Windham-Myers et al. (2018) measured ebullition with a static chamber during 5 days in summer at US-Tw1, and ebullition contributions to the total emission (10-30%) were comparable to those by the current study (26%). In contrast, plant-mediated transport estimated with chambers for FI-Sii (31%) and FI-Si2 (21%) was smaller than our model estimates (91% for FI-Sii and 67% for FI-Si2). However, Susiluoto et al. (2018) reported contributions similar to the current study based on process-based models also constrained using EC data (75%-95%) for FI-Sii. Kwon et al. (2017) measured lower contributions of plant-mediated transport (25%) and ebullition (2%) in RU-Ch2 than the model estimates. McNicol et al. (2017) measured ebullition by bubble traps (<1.3%) and diffusion by dissolved CH<sub>4</sub> (<4.1%) from open water bodies within the flux footprint US-Myb, values which are smaller than the current estimates (18% and 24%, respectively). One reason for the inconsistency might be the spatial heterogeneity at US-Myb. Their study did not consider areas of emergent vegetation where contributions by ebullition can be higher (Villa et al., 2021). Hwang et al. (2020) estimated smaller ebullition (10%-17%) than the current study (61%) based on the wavelet analysis of EC data at KR-Crk. For KR-Crk data in the FLUXNET-CH<sub>4</sub> database, WTD under drainage was provided as 0 cm; thus, the model predicted more saturated conditions at the surface than the actual conditions, resulting in higher contributions by ebullition.

Based on the site-scale validation, iPEACE estimates were consistent with production, ebullition, or diffusive flux observations at two sites, but inconsistent with observations from four sites. A comprehensive validation of estimated transport fluxes is challenging at the site scale owing to limited sites with both EC

data and process studies available at the same location (Table 1). Furthermore, no study has in-situ measured the three transport fluxes simultaneously, resulting in uncertainties in how transport fluxes by process studies are consistent with CH<sub>4</sub> emissions measured with EC towers. Plant-mediated transport could be the priority for in-situ measured transport fluxes to validate CH<sub>4</sub> emissions, since it was estimated to be a major pathway in most sites (Table 2) and in other modeling studies (Table 1). Differences in spatial representativeness between EC towers and process studies could also contribute to inconsistencies.

Our estimated wetland CH<sub>4</sub> emissions were within the range of those measured or predicted with process-based models regardless of difficulties in direct comparisons at the site scale. Although the contributions of each transport flux were highly variable among previous studies (Table 1), plant-mediated transport and ebullition tended to be major transport pathways, consistent with our current estimates (Figure 4). Previous models also estimated plantmediated transport as the major pathway (Table 1), although the VISIT model predicted ebullition as the major pathway for Arctic wetlands (Ito, 2019). In contrast, iPEACE tended to estimate higher contributions from ebullition and lower contributions from diffusion. This difference could be caused by the assumption that ebullition occurs when WTD is greater than 10 cm below the ground (Stanley et al., 2019). The contribution of plant-mediated transport was similar to previous modeling studies because of similar model structure, but tended to be higher than measurements (Table 1). Rhizospheric oxidation (Bansal et al., 2020; Korrensalo et al., 2022) is a potential reason for low CH<sub>4</sub> emissions through vegetation, which was not considered in the current version of iPEACE.

### **Toward refined parameterizations**

Based on the PCA (Figure 7), modeling wetland CH<sub>4</sub> emissions could be improved with refined parameterization and representation of CH<sub>4</sub> production, plant-mediated transport, and diffusion through water. The importance of parameterizations for production and plant-mediated transport was also estimated in a study constraining a global CH<sub>4</sub> model with observed CH<sub>4</sub> emissions at 16 wetland sites (Müller et al., 2015). The high explanatory power in the first PC by the production parameters suggests that CH<sub>4</sub> production was important for inter-site variations in CH<sub>4</sub> emissions. Considering the structure of iPEACE, sites with high  $p_{\rm production}$  could be more limited by substrate availability, whereas sites with high  $Q_{10}$  could be more limited by kinetics. The second PC explained CH<sub>4</sub> emissions that are limited by production and/or transport. A similar trade-off between parameters of production and plant-mediated transport was also inferred in an optimized process-based model (Salmon et al., 2022). These results suggest that a model for explaining variabilities in parameters of production and plant-mediated transport across wetlands is needed for refined simulations rather than determining one set of parameters.

# 4.5 | Next steps in modeling wetland CH<sub>4</sub> emissions

The estimated processes were the most likely processes for explaining observed  $\mathrm{CH_4}$  emissions under the model structure of iPEACE (section 2.2), suggesting that careful interpretation is required. iPEACE considers important processes to explain  $\mathrm{CH_4}$  emissions that have been incorporated in some previous modeling studies (Riley et al., 2011; Walter & Heimann, 2000; Wania et al., 2010). However, definitions and formulations of  $\mathrm{CH_4}$ -related processes are often different among models (Melton et al., 2013). For instance, iPEACE does not include processes included in more mechanistic models (e.g., Salmon et al., 2022; Susiluoto et al., 2018). We need to better define processes in the model and to validate modeled processes, where the model-data fusion could be useful to bridge model and observation.

To improve our understanding of CH<sub>4</sub> emissions from wetlands, future improvements are possible with increased availability of EC data, additional observations, and by incorporating more processes into the model. First, in-situ observations of transport fluxes and production parameters with incubations would be useful to constrain the model because Bayesian optimization can effectively incorporate the additional constraints from observations. Second, more long-term data are required for better constraining the model. The period of the current study ranged from one to 9 years with a median of 4 years. Ueyama et al. (2022) indicated that long-term data (e.g., >3 years) effectively constrained the partitioned fluxes. Furthermore, we did not focus on tree-dominated wetlands (e.g., swamps) owing to the importance of unaccounted processes, such as CH<sub>4</sub> transport to the atmosphere by tree stems (Pangala et al., 2013), or from O<sub>2</sub> transport to the rhizosphere via aerial roots (Purvaja et al., 2004). In this study, we predicted O<sub>2</sub> concentration in the soil based on WTD, but the relationship between O2 concentrations and WTD is complex (Ueyama, Hirano, & Kominami, 2020; Ueyama, Yazaki, et al., 2020). Thus, measurements of WTD and O2 concentrations are strongly recommended for evaluating CH4 emissions in wetlands. The current model considers a 1 m thick soil but anaerobic peat deeper than 1 m could play a role in CH<sub>4</sub> emissions (Peltola et al., 2018; Tokida, Miyazaki, et al., 2007; Tokida, Mizoguchi, et al., 2007). Since flux tower measurements did not continuously monitor the O2 and CH4 concentrations in the deep peat, constraining processes at the deep peat were difficult in this study. Finally, refined modeling wetland CH<sub>4</sub> emission will be possible by evaluating how partitioned emissions are consistent across different models constrained with the same data.

The Bayesian inference in this study might be improved after considering the outlined limitations. We did not obtain reliable results for 6 of 23 sites. The inability could be caused by lack of important processes, but might be resolved with improved mathematical techniques. The error distribution was assumed with Gaussian distribution, which lacked the ability to fit long-tail, such as data containing outliers. Use of other error distributions might improve posterior

inference (Hamura et al., 2022). For 12 sites, at least one chain was not well converged (Figure S1), possibly due to a problem of slow convergence associated with complex multimodal parameter distributions. Introducing Extended Ensemble Monte Carlo (Iba, 2001), such as the replica exchange method, could improve convergence. The techniques for complex parameter distributions could improve the parameter optimization, where some parameters in the current study hit the range of prior distributions (Figure S1) possibly owing to the equifinality problem (Schulz et al., 2001).

#### **ACKNOWLEDGMENTS**

We acknowledge support from the John Wesley Powell Center for Analysis and Synthesis of the U.S. Geological Survey (USGS) ("Wetland FLUXNET Synthesis for Methane" working group, https:// www.usgs.gov/centers/john-wesley-powell-center-for-analy sis-and-synthesis/science/wetland-fluxnet-synthesis), the USGS Ecosystem Mission Area, Land Change Science programs and USGS Water Mission Area, Earth System Processes Division, We thank Dr. Eric J Ward for providing useful comments on the manuscript. ESE was supported by the grants from the Arctic Observatory Program of the National Science Foundation (grant numbers 1936752, 1503912, 1107892) and by the US Geological Survey, Research Work Order 224 to the University of Alaska Fairbanks, the Bonanza Creek Long-Term Ecological Research Program funded by the National Science Foundation (NSF DEB-1026415, DEB-1636476) and the NSF Long-Term Research in Environmental Biology Program (NSF LTREB 2011276). MU was supported by the Arctic Challenge for Sustainability II (ArCS II; JPMXD1420318865) and JSPS KAKENHI (20K21849). AD was supported by US DOE AmeriFlux (7544821). IM was supported by ICOS-Finland (3119871). Academy of Finland project N-PERM and Horizon Europe project GreenFeedBack (101056921). MK was supported by the Rural Development Administration (PJ014892022022). TS was supported by the Helmholtz Association of German Research Centres (VH-NG-821). DE-Zrk is a Terrestrial Environmental Observatories Network (TERENO) site. SB was supported by the U.S. Geological Survey, Ecosystems Mission Area, Land Change Science Program. SG was supported by the SNO Tourbières, CNRS-INSU. OS was supported by the Canada Research Chairs, Canada Foundation for Innovation Leaders Opportunity Fund, and Natural Sciences and Engineering Research Council Discovery Grant Programs. WJR and KYC were supported by the Reducing Uncertainties in Biogeochemical Interactions through Synthesis and Computation (RUBISCO) Scientific Focus Area, Office of Biological and Environmental Research of the U.S. Department of Energy Office of Science. YR was supported by the Ministry of Environment of Korea (2022003640002). Lawrence Berkeley National Laboratory (LBNL) is managed by the University of California for the U.S. Department of Energy under contract DE-AC02-05CH11231, California Department of Water Resources, CA Fish and Wildlife, Delta Stewardship Council and US DOE Ameriflux. Any use of trade, firm, or product names is for descriptive purposes only and does not imply endorsement by the U.S. Government.

362486, O. Downloaded from https://oninelibrary.wiley.com/doi/10.1111/geb. 16594 by University Of Alaka Fairbanks, Wiley Online Library on [2001/2023]. See the Terms and Conditions (https://onlinelibrary.wiley.com/terms-and-conditions) on Wiley Online Library for rules of use; OA articles are governed by the applicable Creative Commons Licensed

## CONFLICT OF INTEREST

The authors declare no conflict of interest.

#### DATA AVAILABILITY STATEMENT

The data that support the findings of this study are available in the FLUXNET-CH<sub>4</sub> Community Product, available at https://fluxnet.org/ data/fluxnet-ch4-community-product/. DOIs for individual site data are provided in Table 2. The iPEACE source code is available upon request to the authors.

#### ORCID

Masahito Ueyama https://orcid.org/0000-0002-4000-4888 Sara H. Knox D https://orcid.org/0000-0003-2255-5835 Kyle B. Delwiche https://orcid.org/0000-0002-5981-2500 Sheel Bansal https://orcid.org/0000-0003-1233-1707 William J. Riley https://orcid.org/0000-0002-4615-2304 Dennis Baldocchi https://orcid.org/0000-0003-3496-4919 Takashi Hirano https://orcid.org/0000-0002-0325-3922 Gavin McNicol https://orcid.org/0000-0002-6655-8045 Lisamarie Windham-Myers Dhttps://orcid. org/0000-0003-0281-9581 Benjamin Poulter https://orcid.org/0000-0002-9493-8600 Robert B. Jackson https://orcid.org/0000-0001-8846-7147 Kuang-Yu Chang https://orcid.org/0000-0002-7859-5871 Jiquen Chen 🔟 https://orcid.org/0000-0003-0761-9458 Housen Chu https://orcid.org/0000-0002-8131-4938 Ankur R. Desai https://orcid.org/0000-0002-5226-6041 Sébastien Gogo 🕩 https://orcid.org/0000-0002-0867-497X Hiroki Iwata https://orcid.org/0000-0002-8962-8982 Minseok Kang (1) https://orcid.org/0000-0003-4901-4465 Ivan Mammarella https://orcid.org/0000-0002-8516-3356 Matthias Peichl https://orcid.org/0000-0002-9940-5846 Oliver Sonnentag https://orcid.org/0000-0001-9333-9721 Eeva-Stiina Tuittila https://orcid.org/0000-0001-8861-3167 Youngryel Ryu https://orcid.org/0000-0001-6238-2479 Eugénie S. Euskirchen https://orcid.org/0000-0002-0848-4295 Mathias Göckede https://orcid.org/0000-0003-2833-8401 Adrien Jacotot https://orcid.org/0000-0002-0126-7597 Mats B. Nilsson https://orcid.org/0000-0003-3765-6399 Torsten Sachs https://orcid.org/0000-0002-9959-4771

## REFERENCES

- Baldocchi, D. (2014). Measuring fluxes of trace gases and energy between ecosystems and the atmosphere—The state and future of the eddy covariance method. Global Change Biology, 20, 3600-3609.
- Bansal, S., Johnson, O. F., Meier, J., & Zhu, X. (2020). Vegetation affects timing and location of wetland methane emissions. Journal of geophysical research. Biogeosciences, 125, e2020JG005777.
- Bohn, T. J., Melton, J. R., Ito, A., Kleinen, T., Spahni, R., Stocker, B. D., Zhang, B., Zhu, X., Schroeder, R., Glagolev, M. V., Maksyutov, S., Brovkin, V., Chen, G., Denisov, S. N., Eliseev, A. V., Gallego-Sala, A., McDonald, K. C., Rawlins, M. A., Riley, W. J., ... Kaplan, J. O. (2015). WETCHIMP-WSL: Intercomparison of wetland methane emissions models over West Siberia. Biogeosciences, 12, 3321-3349.

- Bridgham, S. D., Cadillo-Quiroz, H., Keller, J. K., & Zhuang, Q. (2013). Methane emissions from wetlands: Biogeochemical, microbial, and modeling perspectives from local to global scales. Global Change Biology, 19, 1325-1346.
- Brown, M. G., Humphreys, E. R., Moore, T. R., Roulet, N. T., & Lafleur, P. M. (2014). Evidence for a nonmonotonic relationship between ecosystem-scale peatland methane emissions and water table depth. Journal of Geophysical Research Biogeosciences, 119, 826-835.
- Butterbach-Bahl, K., Papen, H., & Rennenberg, H. (1997). Impact of gas transport through rice cultivars on methane emission from rice paddy fields. Plant, Cell and Environment, 20, 1175-1183.
- Campbell, D., & Goodrich, J. (2020). FLUXNET-CH, NZ-Kop Kopuatai. New Zealand. https://doi.org/10.18140/FLX/1669652
- Castro-Morales, K., Kleinen, T., Kaiser, S., Zaehle, S., Kittler, F., Kwon, M. J., Beer, C., & Göckede, M. (2018). Year-round simulated methane emissions from a permafrost ecosystem in Northeast Siberia. Biogeosciences, 15, 2691-2722.
- Chang, K.-Y., Riley, C., Grant, R. E., & Saleska, S. R. (2020). Hysteretic temperature sensitivity of wetland CH<sub>4</sub> fluxes explained by substrate availability and microbial activity. Biogeosciences, 17, 5849-5860.
- Chang, K.-Y., Riley, W., Knox, S., Jackson, R., McNicol, G., Poulter, B., Aurela, M., Baldocchi, D., Bansal, S., Bohrer, G., Campbell, D., Cescatti, A., Chu, H., Delwiche, K., Desai, A., Euskirchen, E., Friborg, T., Gockede, M., Helbig, M., ... Zona, D. (2021). Substantial hysteresis in emergent temperature sensitivity of global wetland CH<sub>4</sub> emissions. Nature Communications, 12, 2266.
- Chasar, L. S., Chanton, J. P., Glaser, P. H., Siegel, D. I., & Rivers, J. S. (2000). Radiocarbon and stable carbon isotopic evidence for transport and transformation of dissolved organic carbon, dissolved inorganic carbon, and CH<sub>4</sub> in a northern Minnesota peatland. Global Biogeochemical Cycles, 14, 1095-1108.
- Chen, J. (2021). Biophysical models and applications in ecosystem analysis. Michigan State University Press.
- Chen, J., & Chu, H. (2020). FLUXNET-CH<sub>4</sub> US-WPT Winous Point North Marsh, United States. https://doi.org/10.18140/FLX/1669702
- Chen, J., Jönsson, P., Tamura, M., Gu, Z., Matsushita, B., & Eklundh, L. (2004). A simple method for reconstructing a high-quality NDVI time-series data set based on the Savitzky-Golay filter. Remote Sensing of Environment, 91, 332-344.
- Chu, H., Chen, J., Gottgens, J. F., Ouyang, Z., John, R., Czajkowski, K., & Becker, R. (2014). Net ecosystem methane and carbon dioxide exchanges in a Lake Erie coastal marsh and a nearby cropland. Journal of Geophysical Research: Biogeosciences, 119(5), 722-740.
- Conrad, R. (2009). The global methane cycle: Recent advance in understanding the microbial processes involved. Environmental Microbiology Reports, 1, 285-292.
- Delwiche, K. B., Knox, S. H., Malhotra, A., Fluet-Chouinard, E., McNicol, G., Feron, S., Ouyang, Z., Papale, D., Trotta, C., Canfora, E., Cheah, Y.-W., Christianson, D., Alberto, M. C. R., Alekseychik, P., Aurela, M., Baldocchi, D., Bansal, S., Billesbach, D. P., Bohrer, G., ... Jackson, R. B. (2021). FLUXNET-CH<sub>4</sub>: A global, multi-ecosystem dataset and analysis of methane seasonality from freshwater wetlands. Earth System Science Data, 13, 3607-3689.
- Desai, A. R. (2020). FLUXNET-CH<sub>4</sub> US-Los Lost Creek, United States. https://doi.org/10.18140/FLX/1669682
- Dorodnikov, M., Knorr, K.-H., Kuzyakov, Y., & Wilmking, M. (2011). Plant-mediated CH<sub>4</sub> transport and contribution of photosynthates to methanogenesis at a boreal mire: A <sup>14</sup>C pulse-labeling study. Biogeosciences, 8, 2365-2375.
- Eichelmann, E., Knox, S., Rey-Sanchez, A. C., Valach, A., Sturtevant, C., Szutu, D., Verfaillie, J., & Baldocchi, D. (2020). FLUXNET-CH<sub>4</sub> US-Tw4 twitchell east end wetland, United States. https://doi. org/10.18140/FLX/1669698

- Euskirchen, E., Bret-Harte, M., & Edgar, C. (2020). FLUXNET-CH<sub>4</sub> US-ICs Imnavait Creek watershed wet sedge tundra, United States. https://doi.org/10.18140/FLX/1669678
- Euskirchen, E., & Edgar, C. (2020a). FLUXNET-CH<sub>4</sub> US-BZF Bonanza Creek Rich Fen, United States. https://doi.org/10.18140/FLX/1669669
- Euskirchen, E., & Edgar, C. (2020b). FLUXNET-CH $_4$  USBZB Bonanza Creek Thermokarst bog, United States. https://doi.org/10.18140/FLX/1669668
- Glaser, P. H., Morin, C. P., Rosenberry, D. O., Siegel, D. I., Ruud, O., Chasar, L. I., & Reeve, A. S. (2004). Surface deformations as indicators of deep ebullition fluxes in a large northern peatland. Global Biogeochemical Cycles, 19, GB1003. https://doi.org/10.1029/2003G B002069
- Göckede, M., Kittler, F., & Schaller, C. (2019). Quantifying the impact of emission outbursts and non-stationary flow on eddy covariance CH<sub>4</sub> flux measurements using wavelet techniques. *Biogeosciences*, 16, 3113–3131.
- Goeckede, M. (2020). FLUXNET-CH<sub>4</sub> RU-Ch2 Chersky reference. *Russian Federation*. https://doi.org/10.18140/FLX/1669654
- Gogo, S., Guimbaud, C., Laggoun-Défarge, F., Catoire, V., & Robert, C. (2011). In situ quantification of CH<sub>4</sub> bubbling events from a peat soil using a new infrared laser spectrometer. *Journal of Soils Sediments*, 11, 545–551.
- Grant, R. F., Mekonnen, Z. A., Riley, W. J., Arora, B., & Torn, M. S. (2019). Modeling climate change impacts on an arctic polygonal tundra: 2. Changes in CO<sub>2</sub> and CH<sub>4</sub> exchange depend on rates of permafrost thaw as affected by changes in vegetation and drainage. *Journal of Geophysical Research: Biogeosciences*, 124, 1323–1341.
- Hamura, Y., Irie, K., & Sugasawa, S. (2022). Log-regularly varying scale mixture of normals for robust regression. Computational Statistics & Data Analysis, 173, 107517.
- Hoffman, M. D., & Gelman, A. (2014). The No-U-turn sampler: Adaptively setting path lengths in Hamiltonian Monte Carlo. *Journal of Machine Learning Research*, 15, 1593–1623.
- Hwang, Y., Ryu, Y., Huang, Y., Kim, J., Iwata, H., & Kang, M. (2020). Comprehensive assessments of carbon dynamics in an intermittently-irrigated rice paddy. Agricultural and Forest Meteorology, 285-286, 107933.
- Iba, Y. (2001). Extended ensemble Monte Carlo. International Journal of Modern Physics C, 12, 623–656.
- Ito, A. (2019). Methane emission from pan-Arctic natural wetlands estimated using a process-based model, 1901–2016. *Polar Science*, 21,
- lwata, H. (2020). FLUXNET-CH $_4$  JP-Mse Mase rice paddy field. Japan. https://doi.org/10.18140/FLX/1669647
- Iwata, H., Hirata, R., Takahashi, Y., Miyabara, Y., Itoh, M., & Iizuka, K. (2018). Partitioning eddy-covariance methane fluxes from a shallow lake into diffusive and ebullitive fluxes. Boundary-Layer Meteorology, 169, 416-428.
- Iwata, H., Ueyama, M., & Harazono, Y. (2020). FLUXNET-CH4 US-Uaf University of Alaska, Fairbanks: United States. https://doi. org/10.18140/FLX/1669701
- Jackson, R. B., Saunois, M., Bousquet, P., Canadell, J. G., Poulter, B., Stavert, A. R., Bergamaschi, P., Niwa, Y., Segers, A., & Tsuruta, A. (2020). Increasing anthropogenic methane emissions arise equally from agricultural and fossil fuel sources. *Environmental Research Letters*, 15, 071002.
- Jung, M., Reichstein, M., Schwalm, C. R., Huntingford, C., Sitch, S., Ahlström, A., Arneth, A., Camps-Valls, G., Ciais, P., Friedlingstein, P., Gans, F., Ichii, K., Jain, A. K., Kato, E., Papale, D., Poulter, B., Raduly, B., Rödenbeck, C., Tramontana, G., ... Zeng, N. (2017). Compensatory water effects link yearly global land CO<sub>2</sub> sink changes to temperature. *Nature*, 541, 516-520.

- Kajiura, M., & Tokida, T. (2021). Quantifying bubbling emission (ebullition) of methane from a rice paddy using high-time-resolution concentration data obtained during a closed-chamber measurement. Journal of Agricultural Meteorology, 77, 245–252.
- Karofeld, E., & Tónisson, H. (2014). Spatio-temporal changes in bog pool bottom topography – Temperature effect and its influence on pool development: An example from a raised bog in Estonia. *Hydrological Processes*, 28, 958–968.
- Knox, S. H., Bansal, S., McNicol, G., Schafer, K., Sturtevant, C., Ueyama, M., Valach, A. C., Baldocchi, D., Delwiche, K., Desai, A. R., Euskirchen, E., Liu, J., Lohila, A., Malhotra, A., Melling, L., Riley, W., Runkle, B. R. K., Turner, J., Vargas, R., ... Jackson, R. B. (2021). Identifying dominant environmental predictors of freshwater wetland methane fluxes across diurnal to seasonal time scales. Global Change Biology, 27, 3582–3604.
- Knox, S. H., Jackson, R. B., Poulter, B., McNicol, G., Fluet-Chouinard, E., Zhang, Z., Hugelius, G., Bousquet, P., Canadell, J. G., Saunois, M., Papale, D., Chu, H., Keenan, T. F., Baldocchi, D., Torn, M. S., Mammarella, I., Trotta, C., Aurela, M., Bohrer, G., ... Zona, D. (2019). FLUXNET-CH<sub>4</sub> synthesis activity: Objective, observations, and future directions. Bulletin of the American Meteorological Society, 100, 2607–2632.
- Koebsch, F., & Jurasinski, G. (2020). FLUXNET-CH $_4$  DE-Hte Huetelmoor, Germany. https://doi.org/10.18140/FLX/1669634
- Koebsch, F., Jurasinski, G., Koch, M., Hofmann, J., & Glatzel, S. (2015). Controls for multi-scale temporal variation in ecosystem methane exchange during the growing season of a permanently inundated fen. Agricultural and Forest Meteorology, 204, 94-105.
- Korrensalo, A., Mammarella, I., Alekseychik, P., Vesala, T., & Tuittila, E.-S. (2022). Plant mediated methane efflux from a boreal peatland complex. *Plant and Soil*, 471, 375–392.
- Kutzback, L., Wagner, D., & Pfeiffer, E.-M. (2004). Effect of microrelief and vegetation on methane emission from wet polygonal tundra, Lena Delta, northern Siberia. *Biogeochemistry*, 69, 341–362.
- Kwon, M. J., Beulig, F., Ilie, I., Wildner, M., Küsel, K., Merbold, L., Mahecha, M. D., Zimov, N., Zimov, S. A., Heimann, M., Schuur, E. A. G., Kostka, J. E., Kolle, O., Hilke, I., & Göckede, M. (2017). Plants, microorganisms, and soil temperatures contribute to a decrease in methane fluxes on a drained Arctic floodplain. *Global Change Biology*, 23, 2396–2412.
- Lasslop, G., Reichstein, M., Papale, D., Richardson, A. D., Arneth, A., Barr, A., Stoy, P., & Wohlfahrt, G. (2010). Separation of net ecosystem exchange into assimilation and respiration using a light response curve approach: Critical issues and global evaluation. *Global Change Biology*, 16, 187–208.
- Lohila, A., Aurela, M., Tuovinen, J.-P., Laurila, T., Hatakka, J., Rainne, J., & Mäkelä, T. (2020). FLUXNET-CH<sub>4</sub> FI-Lom Lompolojankka, Finland. https://doi.org/10.18140/FLX/1669638
- Ma, S., Jiang, J., Huang, Y., Shi, Z., Wilson, R. M., Ricciuto, D., Sebestyen, S. D., Hanson, P. J., & Luo, Y. (2017). Data-constrained projections of methane fluxes in a northern Minnesota peatland in response to elevated CO<sub>2</sub> and warming. *Journal of Geophysical Research: Biogeosciences*, 122, 2841–2861.
- Mahecha, M. D., Reichstein, M., Carvlhais, N., Lasslop, G., Lange, H., Seneviratne, S. I., Vargas, R., Ammann, C., Arain, M. A., Cescatti, A., Janssens, I. A., Migliavacca, M., Montagnani, L., & Richardson, A. D. (2010). Global convergence in the temperature sensitivity of respiration at ecosystem level. *Science*, 329, 838–840.
- Männistö, E., Korrensalo, A., Alekseychik, P., Mammarella, I., Peltola, O., Vesala, T., & Tuittila, E.-S. (2019). Multi-year methane ebullition measurements from water and bare peat surfaces of a patterned boreal bog. *Biogeosciences*, 16, 2409–2421.
- Matthes, J. H., Sturtevant, C., Oikawa, P., Chamberlain, S. D., Szutu, D., Ortiz, A. A., Verfaillie, J., & Baldocchi, D. (2020). FLUXNET-CH<sub>4</sub> US-Myb Mayberry wetland, United States. https://doi.org/10.18140/ FLX/1669685

- McNicol, G., Sturtevant, C. S., Knox, S. H., Dronova, I., Baldocchi, D. D., & Silver, W. L. (2017). Effects of seasonality, transport pathway, and spatial structure on greenhouse gas fluxes in a restored wetland. Global Change Biology, 23, 2768-2782.
- Melton, J. R., Wania, R., Hodson, E. L., Poulter, B., Ringeval, B., Spahni, R., Bohn, T., Avis, C. A., Beerling, D. J., Chen, G., Eliseev, A. V., Denisov, S. N., Hopcroft, P. O., Lettenmaier, D. P., Riley, W. J., Singarayer, J. S., Subin, Z. M., Tian, H., Zürcher, S., ... Kaplan, J. O. (2013). Present state of global wetland extent and wetland methane modelling: Conclusions from a model inter-comparison project (WETCHIMP). Biogeosciences, 10, 753-788.
- Moore, T. R., & Roulet, N. T. (1993). Methane flux: Water table relations in northern wetlands. Geophysical Research Letter, 20, 587-590.
- Morin, T. H. (2018). Advances in the eddy covariance approach to CH<sub>4</sub> monitoring over two and a half decades. Journal of Geophysical Research: Biogeosciences, 124, 453-460.
- Morrissey, L. A., & Livingston, G. P. (1992). Methane emissions from Alaska Arctic tundra: An assessment of local spatial variability. Journal of Geophysical Research: Atmospheres, 97, 16661–16670.
- Müller, J., Paudel, R., Shoemaker, C. A., Woodbury, J., Wang, Y., & Mahowald, N. (2015). CH<sub>4</sub> parameters estimation in CLM4.5bgc using surrogate global optimization. Geoscientific Model Development, 8, 3285-3310.
- Nilsson, M. B., & Peichl, M. (2020). FLUXNET-CH<sub>4</sub> SE-Deg Degero. Sweden. https://doi.org/10.18140/FLX/1669659
- Pangala, S. R., Moore, S., Hornibrook, E. R. C., & Gauci, V. (2013). Trees are major conduits for methane egress from tropical forested wetlands. New Phytolotist, 197, 524-531.
- Pastorello, G., Trotta, C., Canfora, E., Chu, H., Christianson, D., Cheah, Y.-W., Poindexter, C., Chen, J., Elbashandy, A., Humphrey, M., Isaac, P., Polidori, D., Reichstein, M., Ribeca, A., van Ingen, C., Vuichard, N., Zhang, L., Amiro, B., Ammann, C., & Law, B. (2020). The FLUXNET2015 dataset and the ONEFlux processing pipeline for eddy covariance data. Scientific Data, 7, 225 https://www.nature. com/articles/s41597-020-0534-3
- Peltola, O., Raivonen, M., Li, X., & Vesala, T. (2018). Technical note: Comparison of methane ebullition modelling approaches used in terrestrial wetland models. Biogeosciences, 15, 937-951.
- Purvaja, R., Ramesh, R., & Frenzel, P. (2004). Plant-mediated methane emission from an Indian mangrove. Global Change Biology, 10, 1825-1834.
- Raivonen, M., Smolander, S., Backman, L., Susiluoto, J., Aalto, T., Markkanen, T., Mäkelä, J., Rinne, J., Peltola, O., Aurela, M., Lohila, A., Tomasic, M., Li, X., Larmola, T., Juutinen, S., Tuittila, E.-S., Heimann, M., Sevanto, S., Kleinen, T., ... Vesala, T. (2017). HIMMELI v1.0: Helsinkl model of MEthane buiLd-up and emIssion for peatlands. Geoscientific Model Development, 10, 4665-4691.
- Reichstein, M., Falge, E., Baldocchi, D., Papale, D., Aubinet, M., Berbigier, P., Bernhofer, C., Buchmann, N., Gilmanov, T., Granier, A., Grünwald, T., Havránková, K., Ilvesniemi, H., Janous, D., Knohl, A., Laurila, T., Lohila, A., Loustau, D., Matteucci, G., ... Valentini, R. (2005). On the separation of net ecosystem exchange into assimilation and ecosystem respiration: Review and improved algorithm. Global Change Biology, 11, 1-16.
- Richardson, W. P., Reba, M. L., & Runkle, B. R. (2022). Modification of wavelet-based method for detecting ebullitive methane fluxes in eddy-covariance observations: Application at two rice fields. Boundary-Layer Meteorology, 184, 71-111.
- Riley, W. J., Subin, Z. M., Lawrence, D. M., Swenson, S. C., Torn, M. S., Meng, L., Mahowald, N. M., & Hess, P. (2011). Barriers to predicting change in global terrestrial methane fluxes: Analyses using CLM4Me, a methane biogeochemistry model integrated in CESM. Biogeosciences, 8, 1925-1953.
- Rinne, J., Tuittila, E.-S., Peltola, O., Li, X., Raivonen, M., Alekseychik, P., Haapanala, S., Pihlatie, M., Aurela, M., Mammarella, I., & Vesala, T.

- (2018). Temporal variation of ecosystem scale methane emission from a boreal fen in relation to temperature, water table position, and carbon dioxide fluxes. Global Biogeochemical Cycles, 32, 1087-1106.
- Ryu, Y., Kang, M., & Kim, J. (2020). FLUXNET-CH, KR-CRK Cheorwon Rice paddy. Republic of Korea. https://doi.org/10.18140/FLX/1669649
- Sachs, T., & Wille, C. (2020), FLUXNET-CH, DE-Zrk Zarnekow, Germany, https://doi.org/10.18140/FLX/1669636
- Salmon, E., Jégou, F., Guenet, B., Jourdain, L., Qiu, C., Bastrikov, V., Guimbaud, C., Zhu, D., Ciais, P., Peylin, P., Gogo, S., Laggoun-Défarge, F., Aurela, M., Bret-Harte, M. S., Chen, J., Chojnicki, B. H., Chu, H., Edgar, C. W., ... Ziemblińska, B. (2022). Assessing methane emissions for northern peatlands in ORCHIDEE-PEAT revision 7020. Geoscientific Model Development, 15, 2813-2838.
- Santoni, G. W., Lee, B. H., Goodrich, J. P., Vammer, R. K., Crill, P. M., McManus, J. B., Nelson, D. D., Zahniser, M. S., & Wofsy, S. C. (2012). Mass fluxes and isofluxes of methane (CH<sub>4</sub>) at a New Hampshire fen measured by a continuous wave quantum cascade laser spectrometer. Journal of Geophysical Research, 117, D10301. https://doi. org/10.1029/2011JD016960
- Saunois, M., Stavert, A. R., Poulter, B., Bousquet, P., Canadell, J. G., Jackson, R. B., Raymond, P. A., Dlugokencky, E. J., Houweling, S., Patra, P. K., Ciais, P., Arora, V. K., Bastviken, D., Bergamaschi, P., Blake, D. R., Brailsford, G., Bruhwiler, L., Carlson, K. M., Carrol, M., ... Zhuang, Q. (2020). The global methane budget 2000-2017. Earth System Science Data, 12(3), 1561-1623. https://doi.org/10.5194/ essd-12-1561-2020
- Schaller, C., Kittler, F., Foken, T., & Göckede, M. (2019). Characterisation of short-term extreme methane fluxes related to non-turbulent mixing above an Arctic permafrost ecosystem. Atmospheric Chemistry and Physics, 19, 4041-4059.
- Schmid, H. P., & Klatt, J. (2020). FLUXNET-CH, DE-SfN Schechenfilz Nord, Germany. https://doi.org/10.18140/FLX/1669635
- Schulz, K., Jarvis, A., & Beven, K. (2001). The predictive uncertainty of land surface fluxes in response to increasing ambient carbon dioxide. Journal of Climate, 14, 2551-2562.
- Shannon, R. D., White, J. R., Lawson, J. E., & Gilmour, B. S. (1996). Methane efflux from emergent vegetation in peatlands. Journal of Ecology, 84, 239-246.
- Shortt, R., Hemes, K., Szutu, D., Verfaillie, J., & Baldocchi, D. (2020). FLUXNET-CH, US-Sne Sherman Island restored wetland, United States. https://doi.org/10.18140/FLX/1669693
- Sonnentag, O., & Helbig, M. (2020). FLUXNET-CH, CA-SCB Scotty Creek bog. Canada. https://doi.org/10.18140/FLX/1669613
- Stamp, I., Baird, A. J., & Heppell, C. M. (2013). The importance of ebullition as a mechanism of methane (CH<sub>d</sub>) loss to the atmosphere in a northern peatland. Geophysical Research Letters, 40, 2087-2090.
- Stanley, K. M., Heppell, C. M., Belyea, L. R., Baird, A. J., & Field, R. H. (2019). The importance of CH<sub>4</sub> emission in floodplain fens. Journal of Geophysical Research: Biogeosciences, 124, 1750-1763.
- Sturtevant, C. S., Ruddell, B. L., Knox, S. H., Verfaillie, J., Matthes, J. H., Oikawa, P. Y., & Baldocchi, D. (2016). Identifying scaleemergent, nonlinear, asynchronous processes of wetland methane exchange. Journal of Geophysical Research: Biogeosciences, 121, 188-204.
- Susiluoto, J., Raivonen, M., Backman, L., Laine, M., Peltola, O., Vesala, T., & Aalto, T. (2018). Calibrating the sqHIMMELI v1.0 wetland methane emission model with hierarchical modeling and adaptive MCMC. Geoscientific Model Development, 11, 1199-1228.
- Tokida, T., Miyazaki, T., & Mizoguchi, M. (2005). Ebullition of methane from peat with falling atmospheric pressure. Geophysical Research Letters, 32, L13823. https://doi.org/10.1029/2005GL022949
- Tokida, T., Miyazaki, T., Mizoguchi, M., Nagata, F., Takakai, F., Kagemoto, A., & Hatano, R. (2007). Falling atmospheric pressure as a trigger for methane ebullition from peatland. Global Biogeochemical Cycles, 23, GB2003. https://doi.org/10.1029/2006GB002790

- Tokida, T., Mizoguchi, M., Miyazaki, T., Kagemoto, A., Nagata, O., & Hatano, R. (2007). Episodic release of methane bubbles from peatland during spring thaw. *Chemosphere*, 70, 165–171.
- Turetsky, M. R., Kotowska, A., Bubier, J., Dise, N. B., Crill, P., Hornibrook,
  E. R. C., Minkkinen, K., Moore, T. R., Myers-Smith, I. H., Nykänen,
  H., Olefeldt, D., Rinne, J., Saarnio, S., Shurpali, N., Tuittila, E.-S., Waddington, J. M., White, J. R., Wickland, K. P., & Wilmking,
  M. (2014). A synthesis of methane emissions from 71 northern,
  temperate, and subtropical wetlands. Global Change Biology, 20, 2183–2197.
- Ueyama, M., Hirano, T., & Kominami, Y. (2020). FLUXNET-CH<sub>4</sub> JP-BBY Bibai bog. Japan. https://doi.org/10.18140/FLX/1669646
- Ueyama, M., Yazaki, T., Hirano, T., & Endo, R. (2022). Partitioning methane flux by the eddy covariance method in a cool temperate bog based on a Bayesian framework. *Agricultural and Forest Meteorology*, 316, 8852.
- Ueyama, M., Yazaki, T., Hirano, T., Futakuchi, Y., & Okamura, M. (2020). Environmental controls on methane fluxes in a cool temperate bog. Agricultural and Forest Meteorology, 281, 107852.
- Valach, A., Szutu, D., Eichelmann, E., Knox, S., Verfaillie, J., & Baldocchi, D. (2020). FLUXNET-CH<sub>4</sub> US-Tw1 twitchell wetland west pond. USA. https://doi.org/10.18140/FLX/1669696
- Vesala, T., Tuittila, E.-S., Mammarella, I., & Alekseychik, P. (2020). FLUXNET-CH<sub>4</sub> FI-Si2 Siikaneva-2 Bog. Finland. https://doi.org/10.18140/FLX/1669639
- Vesala, T., Tuittila, E.-S., Mammarella, I., & Rinne, J. (2020). FLUXNET-CH<sub>4</sub> FI-Sii Siikaneva. Finland. https://doi.org/10.18140/FLX/1669640
- Villa, J. A., Ju, Y., Stephen, T., Rey-Sanchez, C., Wrighton, K. C., & Bohrer, G. (2020). Plant-mediated methane transport in emergent and floating-leaved species of a temperate freshwater mineral-soil wetland. *Limnology and Oceanography*, 65, 1635–1650. https://doi.org/10.1002/lno.11467
- Villa, J. A., Ju, Y., Yazbeck, T., Waldo, S., Wrighton, K. C., & Bohrer, G. (2021). Ebullition dominates methane fluxes from the water surface across different ecohydrological patches in a temperate freshwater marsh at the end of the growing season. Science of the Total Environment, 767, 144498.
- Vuichard, N., & Papale, D. (2015). Filling the gaps in meteorological continuous data measured at FLUXNET sites with ERA-interim reanalysis. *Earth System Science Data*, 7, 157–171.
- Walter, P. B., & Heimann, M. (2000). A process-based, climate-sensitive model to derive methane emissions from natural wetlands:

- Application to five wetland sites, sensitivity to model parameters, and climate. *Global Biogeochemical Cycles*, 14, 745–765.
- Wania, R., Ross, I., & Prentice, I. C. (2010). Implementation and evaluation of a new methane model within a dynamic global model: LPJ-WHyMe v1.3.1. Geoscientific Model Development, 3, 565–584.
- Whiting, G. J., & Chanton, J. P. (1993). Primary production control of methane emission from wetlands. *Nature*, 364, 794–795.
- Windham-Myers, L., Bergamaschi, B., Anderson, F., Knox, S., Miller, R., & Fujii, R. (2018). Potential for negative emissions of greenhouse gases (CO<sub>2</sub>, CH<sub>4</sub> and N<sub>2</sub>O) through coastal peatland re-establishment: Novel insights from high frequency flux data at meter and kilometer scales. *Environmental Research Letters*, *13*, 045005.
- Yuan, K., Zhu, Q., Li, F., Riley, W. J., Torn, M. S., Chu, H., McNicol, G., Chen, M., Knox, S. H., Delwiche, K., Wu, H., Baldocchi, D., Ma, H., Desai, A., Chen, J., Sachs, T., Ueyama, M., Sonnentag, O., Helbig, M., ... Jackson, R. (2022). Causality guided machine learning model on wetland CH<sub>4</sub> emissions across global wetlands. Agricultural and Forest Meteorology, 324, 109115.
- Yvon-Durocher, G., Allen, A. P., Bastviken, D., Conrad, R., Gudasz, C., St-Pierre, A., Thanh-Duc, N., & del Giorgio, P. A. (2014). Methane fluxes show consistent temperature dependence across microbial to ecosystem scales. *Nature*, 507, 488–491.

#### SUPPORTING INFORMATION

Additional supporting information can be found online in the Supporting Information section at the end of this article.

How to cite this article: Ueyama, M., Knox, S. H., Delwiche, K. B., Bansal, S., Riley, W. J., Baldocchi, D., Hirano, T., McNicol, G., Schafer, K., Windham-Myers, L., Poulter, B., Jackson, R. B., Chang, K.-Y., Chen, J., Chu, H., Desai, A. R., Gogo, S., Iwata, H., Kang, M. ... Sachs, T. (2023). Modeled production, oxidation, and transport processes of wetland methane emissions in temperate, boreal, and Arctic regions. *Global Change Biology*, 00, 1–22. https://doi.org/10.1111/gcb.16594